LES study of deflagration to detonation mechanisms in a downsized spark ignition engine

A. Robert [a,b,*], S. Richard [a,1], O. Colin [a], T. Poinsot [c]

[a] IFP Energies nouvelles, 1 et 4 avenue de Bois-Préau, 92852 Rueil-Malmaison, France
[b] PSA Peugeot Citroën, route de Gizy, 78943 Velizy-villacoublay, France
[c] IMF Toulouse, Allée du Professeur Camille Soula, 31400 Toulouse, France

ABSTRACT

Using 15 LES cycles of a high load/low speed spark ignition engine operating point, two different fresh gases autoignition regimes called knock and super-knock are analyzed. A direct "a posteriori" analysis of pressure waves and autoignition heat release observed in LES is proposed. It reveals that low to moderate knock intensity, corresponding to late spark timings (ST) is characterized by one or several random autoignition (AI) spots which consume the surrounding fresh gases without coupling with the AI heat release. On the contrary, the highest knock intensities correspond to what is usually called super-knock, a very intense knock observed under pre-ignition conditions or for very early ST, as done in this study. LES shows that the pressure waves generated by one or a couple of AI spots are strong enough to induce locally a strong fresh gases temperature increase leading itself to a substantial decrease of the AI delay. This allows to generate a coupling between the pressure wave and the AI reaction rate which reinforce each other, leading to maximum pressures and propagation speeds close to those of a detonation. These results therefore strongly support the hypothesis proposed in the literature that super-knock is characterized by a deflagration to detonation transition (DDT). An "a priori" analysis is also performed thanks to the use of a local detonation indicator based on Bradley's DDT diagram. It is shown that this tool not only predicts the change of combustion regime as a function of the ST, but it also roughly succeeds in predicting the location and time of appearance of the DDT in the chamber. Unfortunately, the first AI spot is not always responsible for the DDT, implying that using cold flow LES to calculate the detonation indicator instead of a reacting LES as proposed here, would lead to a failure of the indicator in many cases.

Keywords:
LES
Spark ignition
Engine
Knock
Super-knock
Deflagration to detonation transition

1. Introduction

In the last decade, downsized spark ignition (SI) engines running under high loads have become more and more attractive for car manufacturers because of their increased thermal efficiency and lower CO_2 emissions. However, high loads also induce more severe thermodynamic conditions in the cylinder, promoting the occurrence of abnormal combustion phenomena like knock or super-knock.

In a normal cycle, a premixed flame is generated at spark timing (ST) by the spark plug, and its propagation leads to an increase of pressure and temperature of the end gases that are located between the premixed flame front and the cylinder walls. In the case of knock, the autoignition (AI) delay is short enough in part of these fresh gases to allow AI prior to the complete consumption of the fresh gases by the premixed flame. Knock therefore highly depends on the premixed flame combustion velocity as well as on species composition and temperature fluctuations in the cylinder, which all influence the autoignition delays, making knock a recurrent but non-cyclic phenomenon. The experimental study of such phenomenon is difficult but some attempts are available in the literature [1]. On the other hand, pre-ignition, also called LSPI (Low Speed Pre-Ignition) [2] corresponds to the autoignition of a fresh gases spot before ST that acts as a spark plug itself, leading to the creation of a premixed flame before ST. A pre-ignition cycle can be schematically understood as a cycle experiencing a very early ST as experimentally shown in [2]. As the premixed flame develops earlier in a pre-igniting cycle (or with a very early ST), autoignition of the end gas is often observed, but not

* Corresponding author at: IFP Energies nouvelles, 1 et 4 avenue de Bois-Préau, 92852 Rueil-Malmaison, France. Fax: +33 147526685.
E-mail address: anthony.robert@ifpen.fr (A. Robert).
[1] Now, at SAFRAN Turbomeca.

systematically [3,4]. If this autoignition event is weak, it is similar to knock under standard spark ignition, this is why it is still called knock. On the contrary, extremely strong autoignitions can be observed at a very low frequency, leading to a fast and intense pressure rise [2–4]. Physically, this means that a large amount of fresh gases autoignites suddenly, leading to extreme pressure levels reaching several hundred bars. These extreme knock events are called super-knock.

Flame speeds between 1 and 2 km/s were measured in some specific super-knock operating conditions [5,6], which are at least two orders of magnitude larger than the turbulent premixed flame speed. Besides, the pressure levels recorded by pressure transducers indicate that the pressure rise can be sometimes larger than the constant volume pressure increase observed in a homogeneous autoignition [4]. These observations suggest that super-knock is characterized by a deflagration to detonation transition (DDT). As super-knock causes the rapid destruction of the engine, and is extremely fast (a couple of crank angle degrees (CAD)), a detailed experimental investigation is nearly impossible.

This motivated the use of CFD for better understanding knock and super-knock. RANS simulations were used to predict and understand the occurrence of knock [7–9] and super-knock [10]. However the RANS approach is limited to the description of the mean cycle, which is not necessarily subjected to knock or super-knock because of their sporadic nature. New approaches have been developed for the study of DDT in piston engines thanks to the use of probability functions to extract knock statistics from RANS simulations [11,12]. A direct analysis of DDT still remains difficult to achieve in RANS because all variables correspond to a mean engine cycle which does not provide local time-resolved informations.

Large Eddy Simulation (LES) appears as an attractive alternative because it allows the simulation of individual cycles, thus reproducing the sporadicity of abnormal combustions. Our recent study [13] shows that LES can capture knock characteristics (frequency of occurence, intensity) over a wide range of ST. In addition, an exponential increase of knock intensity was observed at the earliest ST, suggesting the occurence of a DDT as previously mentioned but without clear evidence.

The present paper focuses on the mechanisms leading to detonation, when going from standard knock to super-knock, using LES for a high load/low speed operating point presented in [13]. The LES models employed and knock statistics obtained for this operating point are briefly presented in Section 2 along with comparisons to experimental data.

A first a priori analysis is performed in Section 3 applying the theoretical DDT indicator proposed by Bradley and coworkers [14–17] to LES fields. Then, an a posteriori analysis of the existence of a DDT is performed in Section 4 using the pressure waves and autoignition heat release from the LES fields. Three operating points with ST representative of moderate, strong and super-knock are analyzed using different cycles to highlight the large cycle-to-cycle variability of autoignition phenomena in piston engines.

2. Quantification of knock using LES

2.1. LES model and solver

The AVBP compressible and reactive LES solver co-developed by IFPEN and CERFACS [18] was used in this study. The premixed turbulent flame is described by the flame surface density model ECFM-LES [19] and the spark ignition model ISSIM [20]. Focusing on mesh resolution, the cell size is close to 0.8 mm in the combustion chamber almost over the whole cycle. Indeed, during combustion, the cell size is of the order of 0.2 mm around the spark plug and 0.5 mm in the rest of the chamber. With such a mesh resolution, previous studies [13,19] have shown that the bimodal description of the ECFM model coupled to a flame surface density equation, allows to describe the premixed flame accurately.

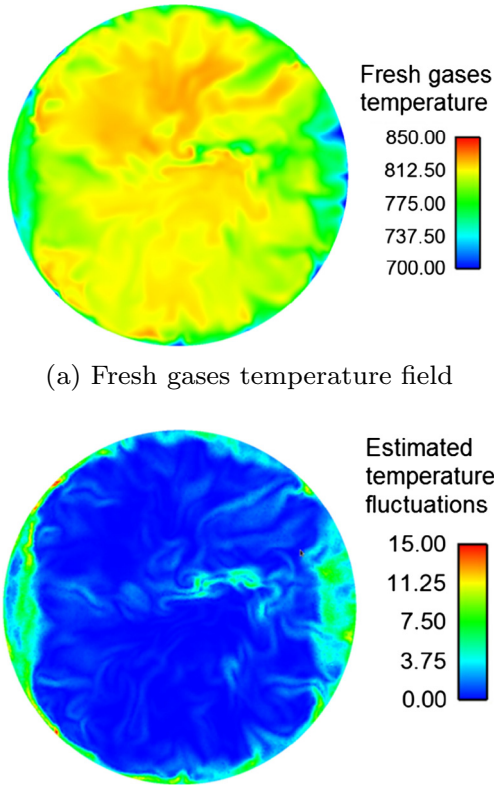

(a) Fresh gases temperature field

(b) Estimated temperature fluctuations [22]

Fig. 1. Fresh gases temperature field (a) and estimated temperature fluctuations [22] (b) at an instant close to the autoignition start.

The autoignition reaction rate is given by the tabulated autoignition model TKI (Tabulated Kinetics of Ignition) [21]. A uniform mixture state is assumed in the autoigniting zone (see [13] for a description of the autoigniting zone). This hypothesis is justified by the fact that mixture fraction is constant and that fresh gases temperature fluctuations are relatively small: using an algebraic expression [22] based on LES fresh gases temperature field (Fig. 1a), fluctuations are estimated below 8 K (Fig. 1b). Local autoignition without propagation is consequently considered well resolved by the LES.

First simulations performed with both ECFM-LES and TKI [23] showed that the premixed flame and autoignition phenomena were not fully decoupled. This is why the present LES were performed with improved versions of ECFM-LES, ISSIM and TKI models proposed in [13]. In this version, the autoignition and flame propagation are described by two independent progress variables $\tilde{c}_{ai}$ and $\tilde{c}_{\Sigma}$ that allow a full decoupling of both phenomena. The interested reader will find the details of this improved version in [13].

In the case of a transition from deflagration to detonation, a stiff autoigniting front develops whose thickness can be as thin as a few molecular free pathes. It cannot be resolved by any piston engine LES of reasonable mesh resolution. At the same time, a detonation follows jump conditions like a shock which are given by Chapman–Jouguet relations. As these jump conditions are naturally described by Navier Stokes equations, it can be expected that the present LES correctly reproduce the transition to detonation.

2.2. Knock statistics from LES

The operating point computed here corresponds to the high load/low speed operating point of [13], summarized in Table 1.

A spark timing sweep has been simulated using LES for seven different spark timings. Performing a multi-cycle simulation for each ST would represent 105 cycles (15 cycles per ST), which is quite expensive in the perspective of an industrial usage of LES. Considering that the flow and combustion of a given cycle have a low impact on the following cycle in SI 4-stroke engines [19] due to the uncoupling of intake and exhaust phases, we propose a specific strategy to limit the CPU time. As the different ST simulated have the same operating conditions (in terms of engine speed and load), we consider that the 15 LES consecutive cycles with the reference ST provide independent initial conditions (corresponding to fields of velocity, energy and mass fraction at ST CAD) for the other ST. This way, only the combustion phases of each cycle are simulated by just changing the ST. CPU time is then reduced by more than twice, which makes the ST variation much cheaper.

For all these ST, it was shown [13] that LES is able to capture the in-cylinder pressure envelope recorded at the cylinder head, as illustrated in Fig. 2 for a ST of 6 CAD. The 15 LES cycles (black) agree well with the 500 experimental cycles (brown[2]) in terms of pressure level and knock occurrence as pressure oscillations characterizing this phenomenon are only present for cycles presenting a fast propagative combustion (i.e. cycles in the upper part of the pressure envelope). It is important to notice that the cycle-to-cycle variations are only due to the intermittency of turbulence in the combustion chamber from one cycle to the other, as already observed on a different engine in Vermorel et al. [19]. LES and experiment also agree in terms of the angle of knock appearance and the percentage of knock occurrence at all ST values.

The maximum knock intensity is presented in Fig. 3a for the experimentally available ST. This intensity is calculated both for experiments and LES using a numerical filtering algorithm of the local in-cylinder pressure signal:

- Only the combustion stroke pressure signal is considered for the analysis.
- A filtering is applied on the characteristic range of knock frequencies [5–9 kHz] using a high pass and a low pass Butterworth filter [25].
- The obtained signal is then rectified and post-processed using a low-pass filter.
- Finally, the knock intensity is given by the maximum of the previously filtered signals for each cycle, it is thus expressed as a pressure variation in bars.

LES predicts correct levels of maximum intensities, and captures the intensity increase as the spark timing decreases. Figure 3b presents the same quantity for all the spark timings computed in LES. When the spark timing occurs before Top Dead Center (bTDC), an exponential increase of the maximum intensity is observed, which suggests complex combustion behavior. This phenomenon is well known, but still misunderstood.

Engine manufacturers are used to correlate knock intensity with the Burned Mass Fraction (BMF) by autoignition [26,27], using a linear relationship between these two quantities. The same analysis is carried out here using the LES results, and Fig. 4 presents the evolution of the maximum knock intensity against the percentage of mass burned by AI. The linear correlation is confirmed by LES,

[2] For interpretation of color in Fig. 2, the reader is referred to the web version of this article.

Table 1
Engine features and operating conditions.

Engine features	Single cylinder
Cylinder capacity (cm^3)	400
Dead volume (cm^3)	42.2
Bore (mm)	77
Stroke (mm)	85.8
Conrod (mm)	132.2
Compression ratio	10.64
Operating point	Knock
RPM (r/min)	1800
IMEP (bar)	19
Intake pressure (bar)	1.802
Intake temperature (K)	308.05
Spark timings	−4 CAD to 15 CAD aTDC
Fuel	Isooctane
Chemical mechanism for TKI table	Jerzembeck [24]

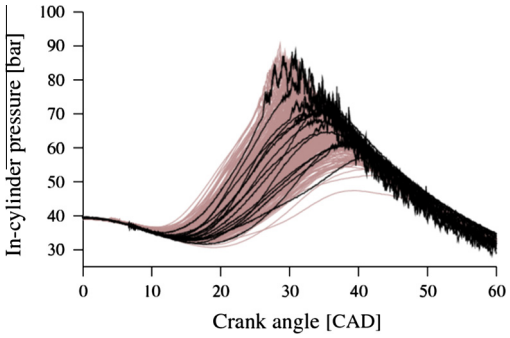

Fig. 2. Local in-cylinder pressure with a spark ignition at 6 CAD aTDC [13].

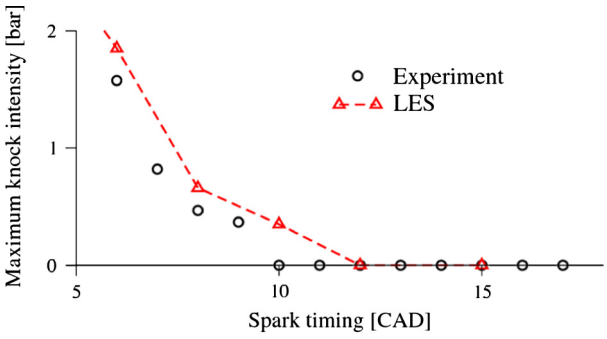

(a) Focus on common ST between LES and experiment

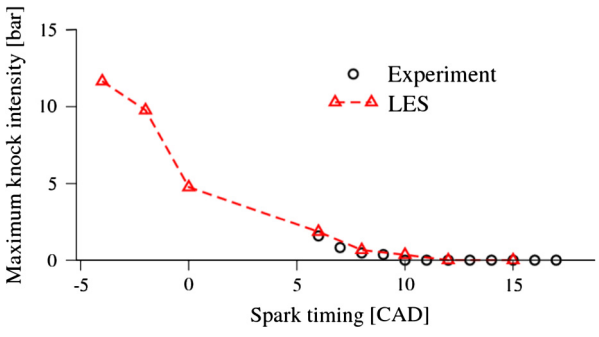

(b) Full ST sweep

Fig. 3. Maximum intensity of knocking cycles on the spark timing sweep [13].

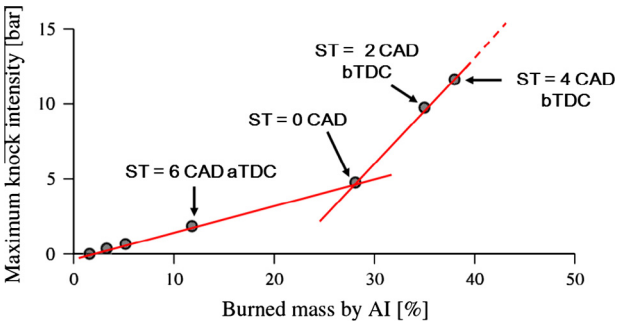

Fig. 4. Evolution of the maximum knock intensity over the percentage of mass burned by autoignition for the LES spark timing sweep.

with a knock intensity proportional to the mass burned by AI below a knock intensity of 4.5 bar. However, LES shows a second regime at the earliest ST, which is characterized by a faster increase of the knock intensity. For the present conditions, this regime appears approximately for ST at and before Top Dead Center (bTDC).

2.3. Definition of the knock regimes

Based on Figs. 3 and 4, three levels of knock intensity can be identified as proposed in Table 2. The latest ST leads to a low knock intensity which is qualified as "trace to moderate knock", and roughly corresponds to the maximum acceptable knock level in a production SI engine. Another regime is qualified as "strong knock" for cases with a maximum intensity comprised between 1 and 5 bars, and a knock frequency around 50%. This regime extends from ST = 6 to 0 CAD after Top Dead Center (aTDC). ST at TDC therefore corresponds to a threshold point between the strong knock regime and the third one. In this last regime, corresponding to ST of 2 and 4 CAD bTDC, the premixed flame propagation happens very early in the cycle and is followed by the most intense knock events. As discussed in the introduction, these features are characteristic of a pre-ignition followed by super-knock, although here they are not obtained through a pre-ignition of a fresh gases hot spot, but through a very early ST, as experimentally done by Amann et al. [2]. This last regime is consequently called 'super-knock" regime.

3. Deflagration to detonation transition analysis using Bradley's diagram

Several authors in the literature have discussed the possible relation between strong knock events and deflagration to detonation transition (DDT) in super-charged SI engines [11,12,14,15,28,29]. The strong increase of knock intensity at the earliest ST could be explained by such a transition, leading locally to very high pressure levels in the combustion chamber. However, this statement has never been demonstrated as it is a high frequency phenomenon difficult to visualize in a real engine test bench, and numerical tools like RANS were not able to represent it.

Based on the LES results of Robert et al. [13], an a priori analysis of DDT using Bradley's diagram [14] is proposed here.

3.1. Bradley's theory on DDT

According to Zel'dovich classification of combustion regimes [30], two conditions seem to be necessary to initiate a coupling between pressure waves and an AI front: a smooth temperature gradient in the fresh gases surrounding the initial AI spot, and an AI propagation velocity close to the sound speed. Based on these observations, Bradley and Morley [14] proposed two parameters representing the coupling conditions of a DDT. The first parameter ε is given by:

$$\varepsilon = \frac{l/a}{\tau_e} \tag{1}$$

with l the length over which the temperature gradient is considered as constant. In the present LES, l is fixed as a first approximation equal to 1 cm thanks to a priori visualizations of instantaneous LES temperature fields at the AI start timing. As will be shown below, even if l is not known with good accuracy, a qualitative exploitation of Bradley's diagram is still possible. "a" is the sound speed and τ_e the excitation time which represents the time to go from 5% to the maximal heat release. In LES, the excitation time is computed using the inverse of the maximum of the AI reaction rate extracted from the TKI table at the thermodynamic conditions considered. This non-dimensional parameter ε compares the time for the pressure wave to travel for a distance l to the excitation time. It allows to determine if the AI can feed the pressure wave and lead to an increase of its amplitude.

A second non-dimensional parameter ξ is proposed to compare the AI and pressure wave propagation velocities. These two velocities have to be of the same order to expect that a coupling mechanism takes place. The AI velocity is defined as the inverse of a delay gradient $\frac{\partial \tau}{\partial x}$, and the parameter ξ is expressed as:

$$\xi = \frac{a}{u} = a\frac{\partial \tau}{\partial x} \tag{2}$$

where u is the apparent autoignition propagation speed. In the original analysis of Bradley, $u^{-1} = \frac{\partial \tau}{\partial x}$ is calculated as the derivative of the complete AI delay from $c_{ai} = 0$ and $c_{ai} = 1$. In the present LES calculations, a more accurate expression is used, considering the delay between the current value of $\tilde{c}_{ai}$ at the point considered and the value $c_{ai} = 0.5$.

Based on these two parameters, Bradley and Morley [14] proposed a (ε, ξ) diagram to locate the developing detonation peninsula. As seen in Fig. 5a, three regimes can be established. In the deflagration zone $(\xi > \xi_u)$, a classical flame propagation is observed, and no coupling occurs with the pressure wave. In the thermal explosion zone $(0 < \xi < \xi_l)$, all fresh gases remaining in the combustion chamber autoignite at the same time due to a negligible temperature gradient. Finally in the developing detonation zone $(\xi_l < \xi < \xi_u)$, a coupling between pressure waves and autoignition is observed, that is, a DDT can be observed. This diagram is now applied to the LES presented in the previous chapter, using the approximated expressions of ξ_l and ξ_u given by Peters et al. [12].

3.2. Application to the LES cycles

The values of ε and ξ calculated at various grid points of the above LES are placed on Bradley's diagram in Fig. 5 for different

Table 2
Classification of knock intensity for the several ST of the chosen engine configuration.

Spark timing	−4	−2	0	6	8	10
Knock	Super-knock		Strong knock		Trace/moderate knock	

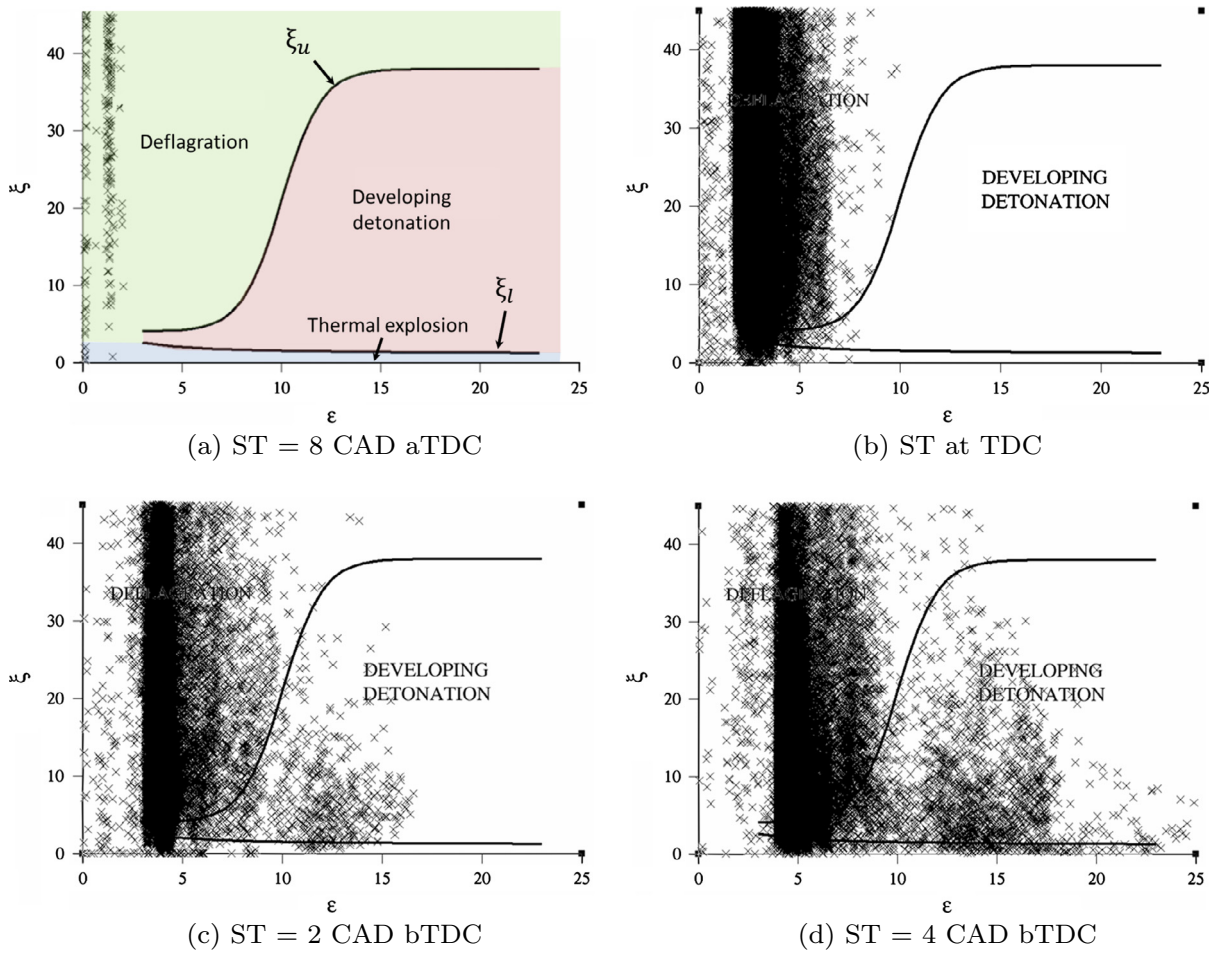

(a) ST = 8 CAD aTDC (b) ST at TDC

(c) ST = 2 CAD bTDC (d) ST = 4 CAD bTDC

Fig. 5. Scatterplot of grid nodes close to autoignite in the detonation diagram.

ST. For each ST, the values are displayed over the whole 15 combustion strokes but to improve the readability of the figure, only grid points which are close to the autoignition delay (i.e. points with an AI progress variable c_{ai} comprised between 0.1 and 0.9) are represented. This selection criterion allows to suppress points which are not autoigniting ($c_{ai} < 0.1$) and points where AI is already over ($c_{ai} > 0.9$). At ST = 8 CAD aTDC (Fig. 5a), only a few points appear in the graph meaning that only a very small fraction of the fresh gases volume is close to autoignite in the cylinder. In addition, these nodes are clearly in the deflagration zone.

Figure 5b confirms that the ST at TDC is a transitional point. A higher number of points are close to autoignite, and some of them are in the transition zone between deflagration and detonation. The tendency of moving from deflagration to detonation zones when ST decreases is confirmed by Fig. 5c and d, which are respectively at ST = 2 and 4 CAD bTDC. When ST decreases more and more grid points are close to AI, and the large amount of points located in the detonation zone for ST = 4 CAD bTDC confirms that a DDT could be responsible for the high knock intensities recorded at this ST.

Based on Bradley's theory, the diagrams of Fig. 5 give an a priori overview of the possible existence of a DDT which seems in good agreement with the evolution of knock intensity with ST. This agreement is in our opinion largely due to the usage of LES fields to compute parameter ξ: in LES, the spatial gradient of the delay is computed from the composition and temperature field of a real cycle while in RANS, it becomes extremely difficult to decorrelate which part of the temperature gradient is due to cycle-to-cycle fluctuations (which should not enter in the calculation of the two parameters) and which part is due to spatial gradients. The situation is even worse in the experiment where it is extremely difficult to measure a three dimensional temperature field.

Unlike ξ, ε is not known precisely as the length scale l (see Eq. (1)) is assumed constant. At the same time, if l is divided by a factor two (going from 1 cm to 0.5 cm), many points would remain in the detonation peninsula, i.e., the interpretation of the diagram would remain essentially identical. Consequently, the essential information that should be considered is not the exact position on the ε axis, but the amplitude of the displacement towards the right of the diagram, from the deflagration to the detonation zone. This shows that such a diagram can predict the global transition towards the DDT region, but its accuracy is too limited to quantitatively predict the ST at which this transition will occur. For this reason, a direct analysis is proposed in the next section.

4. Direct analysis of interactions between autoignition spots and pressure waves

The previous section has shown that DDT conditions could possibly be encountered at the earliest ST using a theoretical criterion. But this criterion remains "a priori" because it does not prove the existence of the DDT, and it is based on strong assumptions whose validity might be questionable under piston engine conditions. The main limitations are listed below:

- As discussed in the previous section, l is difficult to estimate. Peters et al. [12] proposed a sophisticated method to calculate l for their DNS, but it would greatly increase the CPU cost of LES.
- The limits of the detonation peninsula are not universal and should only be considered as transition regions from one regime to the other. Profiles are based on equi-mole CO–H_2 calculations, and Rudloff et al. [28] showed that the chemical mechanism used to solve chemistry can have a non-negligible impact especially on the estimation of the ε parameter.
- As shown below, the pressure wave/heat release interaction takes place in a complex 3D field, which is far from the hypothesis of a 1D DNS used to compute the diagram of Bradley.
- As shown below, the first AI spot is not necessarily responsible for the DDT. It happens that a first AI spot can trigger, due to the pressure it generates, a secondary spot which will be responsible for the DDT. This means that extracting ξ and ε from a cold flow LES will not necessarily allow a correct prediction of DDTs. In other words, the present success of Bradley's diagram to predict DDT is also partly due to the fact that it is based on a reactive LES that already provides explicitly the pressure wave/heat release interactions.

However, independently from this criterion, the simultaneous calculation of the premixed flame propagation with ECFM-LES and autoignition with TKI-LES allows a direct analysis of the interactions between pressure waves and AI heat release. Such an analysis can be used to confirm the occurence of DDT, and the applicability of Bradley's theory to knocking combustion in practical applications.

This section therefore proposes to directly visualize the pressure waves in the combustion chamber and their interactions with AI spots. Based on Table 2, three cases with different ST (4 CAD bTDC, 0 and 8 CAD aTDC) are presented, giving an overview of the possible interactions during moderate, strong and super-knock cycles. For each case, two cycles are analyzed thanks to observations performed every 0.02 CAD (or 1.85 µs). Pressure waves are tracked on a horizontal plane thanks to the visualization of the local pressure difference relative to the mean chamber pressure (and called ΔP afterwards).

In order to evaluate the ability of Bradley's parameters to locate in space and time the occurence of a DDT, we need to visualize simultaneously the two parameters ξ and ε on 2D planes, which is not an easy task. For this reason, a detonation indicator called $\mathbb{R}$ is proposed in this study (Eq. (5)). It is defined as the product of two efficiency functions η_ε and η_ξ, as defined in Eqs. (3) and (4) respectively. These functions are themselves built to equal unity in the DDT peninsula, which is defined approximately by $\varepsilon \geqslant 10$ and $5 < \xi < 40$, and zero elsewhere:

$$\eta_\varepsilon = \frac{1}{2}(\tanh(\varepsilon - 10) + 1) \tag{3}$$

$$\eta_\xi = \frac{1}{2}(\tanh(\xi - 5) - \tanh(\xi - 40)) \tag{4}$$

$$\mathbb{R} = \eta_\varepsilon \eta_\xi \tag{5}$$

4.1. Moderate knock

In this section, a single cycle (cycle 6) is detailed in terms of pressure/autoignition waves interactions. Figure 6 presents its pressure trace at the location of the experimental pressure sensor, the burned mass fraction and the total fuel reaction rate from the premixed flame and from autoignition. The three quantities indicate that combustion starts in a purely propagative mode. For comparison, another cycle, cycle 7, is also presented, showing a faster propagation. The fuel reaction rate by autoignition becomes non negligible after 20 CAD aTDC for both cycles, but it still corresponds to very small values of the progress variable c_{ai} in this period. The formation of a burned gases spot by autoignition ($c_{ai} = 1$) corresponds to the AI reaction rate peak observed at 31.3 CAD for cycle 6 and at 34.6 CAD for cycle 7. The reaction rate peak is also more intense for cycle 6, as confirmed by the larger pressure fluctuations observed for this cycle. Although cycle 6 presents a more intense knock compared to cycle 7, in both cases the pressure fluctuations are limited to a few bars which corresponds to a trace to moderate knock.

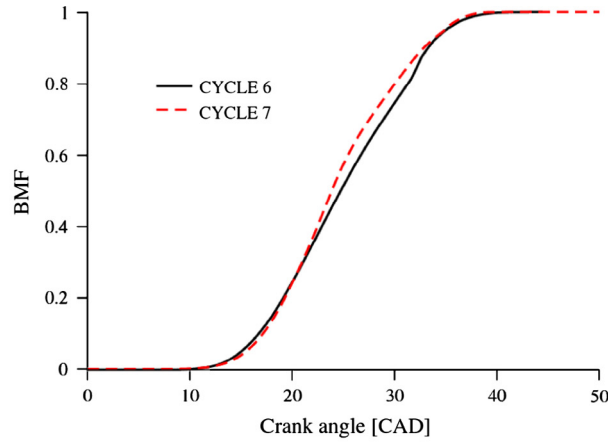

(a) Burned mass fraction

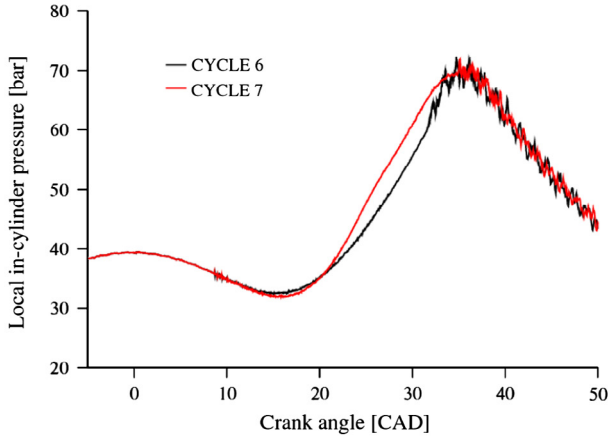

(b) Local in-cylinder pressure

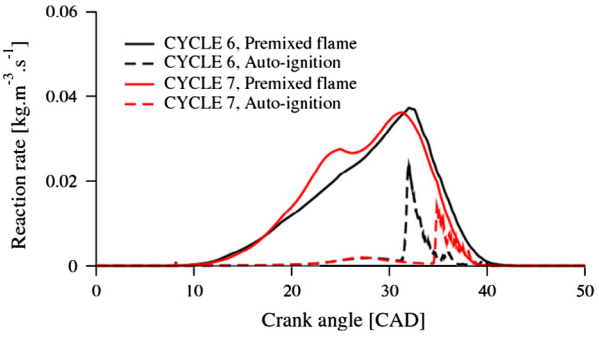

(c) Fuel reaction rates

Fig. 6. Burned mass fraction, local in-cylinder pressure and reaction rate evolutions for the LES cycles 6 and 7 at the ST = 8 CAD aTDC.

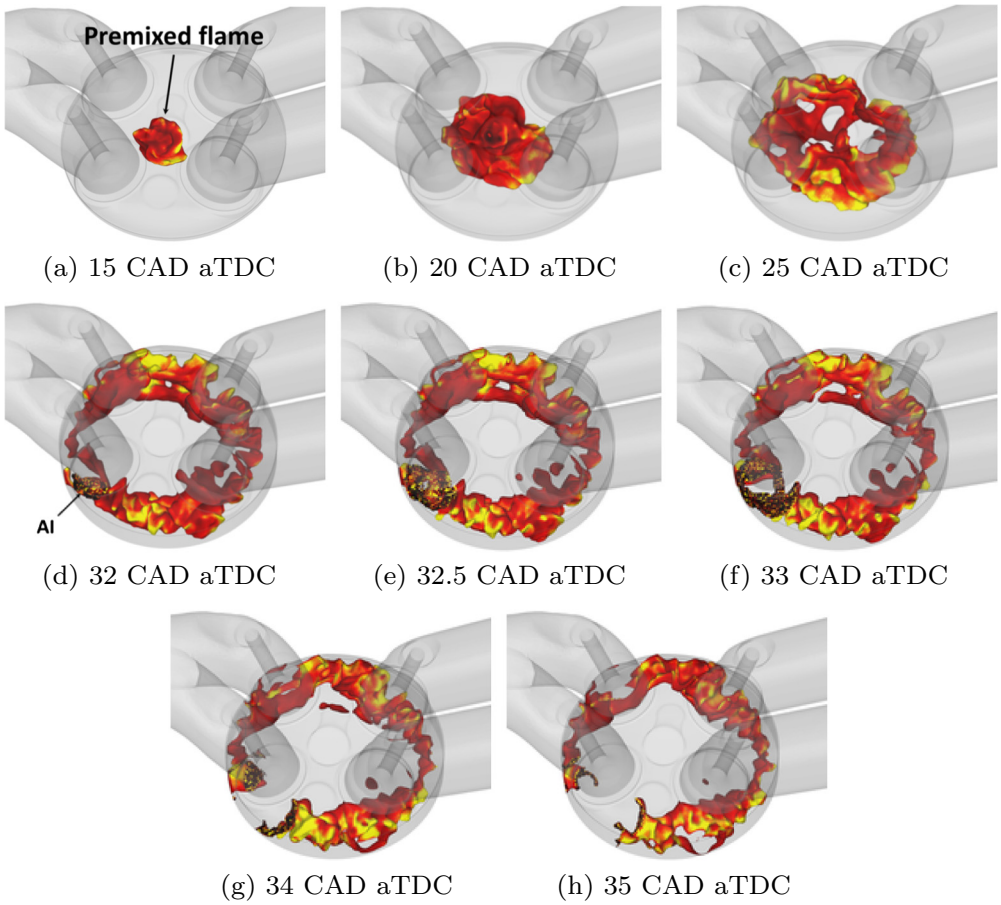

Fig. 7. Evolution of 3D isosurfaces of $\tilde{c}_\Sigma$ (yellow/red), and c_{ai} (black) for cycle 6 at ST = 8 CAD aTDC. (For interpretation of the references to color in this figure legend, the reader is referred to the web version of this article.)

4.1.1. Analysis of cycle 6

The formulation used to express independently the two progress variables c_Σ for ECFM-LES and c_{ai} for TKI-LES allows to follow the premixed flame propagation and the autoignition spot development using isosurfaces of the progress variables c_Σ (yellow/red) and c_{ai} (black). Figure 7 shows the evolution of these two phenomena from spark ignition to the end of AI. After sparking, the premixed flame grows normally in the chamber (Fig. 7a–c). The first AI spot appears at 32 CAD aTDC (Fig. 7d), when a large part of the fuel has been consumed by the propagative flame confirming the value of about 80% of burned mass fraction at this instant (Fig. 6a). This AI spot consumes the pocket of fresh gases that surrounds it, and vanishes at 35 CAD aTDC (Fig. 7h) with a propagation zone limited to a few centimeters around the initial location. The remaining fresh gases are consumed by the premixed flame.

The previous analysis points out that no coupling between premixed flame propagation and AI takes place during this cycle, and that only local AI spots can be observed. To better analyze the underlying physics, Fig. 8 presents the local pressure fluctuation $\Delta P = P(x) - P_{chamber}$ (left column), the fresh gases temperature (middle) and the AI delay (right column) evolutions for instants where a premixed flame and AI spots coexist in the combustion chamber. The premixed flame position is followed thanks to an isoline of the progress variable c_Σ (red), whereas the AI front is localized using an isoline of the AI progress variable c_{ai} (black). Looking at the pressure evolution over time (left column), pressure waves are generated by an AI spot at 32 CAD aTDC (Fig. 8a), and are reflected against the wall of the combustion chamber (Fig. 8b–d). These pressure fluctuations are very limited in magnitude (of the order of 1 bar), and correspond to the pressure signal fluctuations recorded by the pressure sensor at the cylinder head (Fig. 6b). Looking at the fresh gases temperature and AI delay, Fig. 8a shows that AI starts in the region where the fresh gases temperature is the highest, and increases their temperature by about 15 K. However, Fig. 8a–d confirm that the pressure wave propagation leads to a very limited increase of the fresh gases temperature, which is not sufficient to lower significantly the autoignition delay which remains close to 5 CAD. This explains why AI remains located close to the initial spot.

The detonation indicator $\mathbb{R}$ remains equal to zero in the whole chamber and at any time (not presented here). For this case, no coupling is detected, in coherence with the above direct visualization and with the scatter plots of Fig. 5a. In conclusion, both tools confirm that this cycle is in the deflagration zone. AI spot emits a pressure wave which travels in the cylinder quicker than the AI front, but its limited amplitude does not reduce the AI delay sufficiently to ensure a rapid propagation of an autoignition front, and the occurrence of a DDT.

4.1.2. Conclusions for a spark timing at 8 CAD aTDC

Other cycles at this ST were analyzed and presented the same scenario with one or several AI spots as for cycle 6. It can be concluded that although cyclic variability leads to fluctuations in the premixed flame propagation speed, angle of knock onset and knock intensity, all cycles present a low level of pressure fluctuations and no coupling between the generated pressure waves and autoignition. These conclusions confirm the a priori observations drawn using the graph representing the maximal intensity versus burned

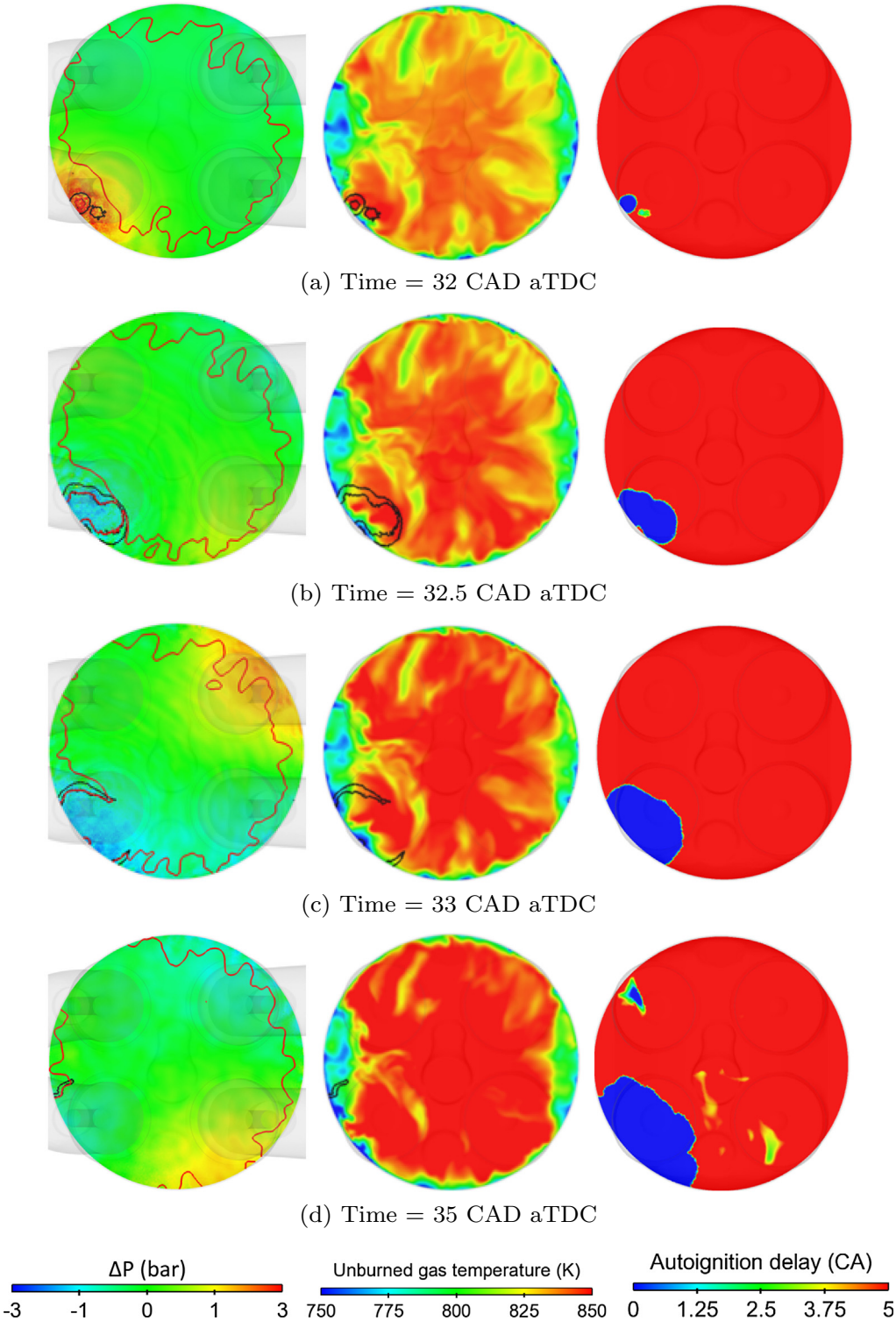

Fig. 8. ΔP evolution (left), fresh gases temperature (middle) and autoignition delay (right) at several instants for cycle 6 at ST = 8 CAD aTDC (Red line: isoline of c_Σ; Black line: isoline of c_{ai}). (For interpretation of the references to color in this figure legend, the reader is referred to the web version of this article.)

mass fraction by AI (Fig. 4) and the scatter plots in Bradley's diagram (Fig. 5). Finally, the proposed detonation indicator remains equal to zero for all cycles, in agreement with Bradley's diagram.

4.2. Transition from strong knock to super-knock

The operating point where spark timing takes place at TDC is now analyzed. For this regime, knock is expected. Two LES cycles are selected among the fifteen available (cycles 6 and 8), and the combustion development is compared using the burned mass fraction (Fig. 9a), the local in-cylinder pressure sensor (Fig. 9b), and the fuel reaction rate (Fig. 9c). These figures show that cycle 6 presents a faster premixed flame combustion compared to cycle 8. The knock onset is also observed earlier for cycle 6 (at 18.6 CAD aTDC) compared to cycle 8 (at 23.7 CAD aTDC). As the autoignition peak reaction rate is approximately

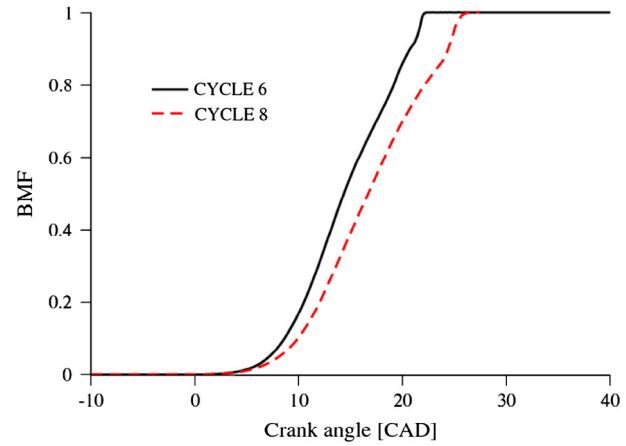

(a) Burned mass fraction over CAD

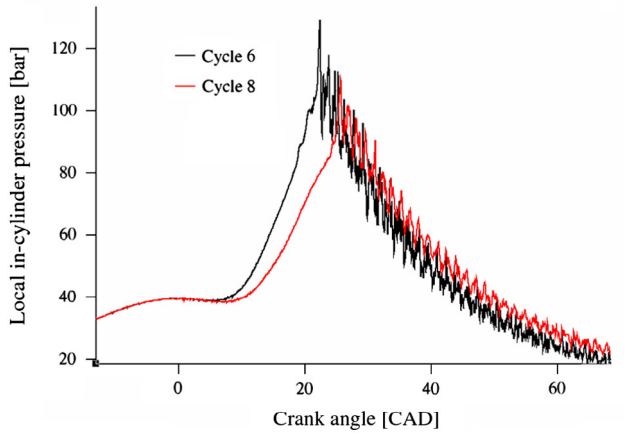

(b) Local in-cylinder pressure over CAD

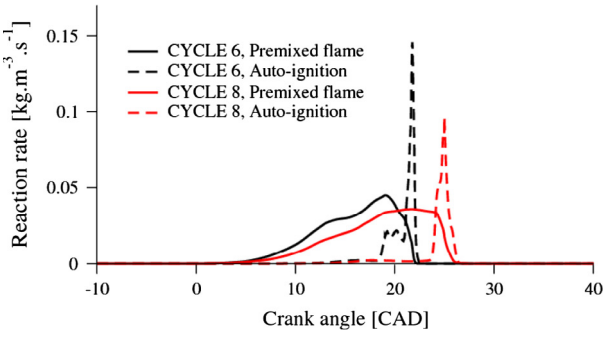

(c) Fuel reaction rates over CAD

Fig. 9. Burned mass fraction, local in-cylinder pressure and reaction rate evolutions for the LES cycles 6 and 8 at the ST = 0 CAD.

eight times larger than at ST = 8 CAD aTDC, a rapid increase in the slope of the burned mass fraction at knock onset is more clearly observed for this case. The local in-cylinder pressure (Fig. 9b) confirms the difference of combustion velocity between these two cycles, with faster pressure rise for cycle 6. The intensity of knock also seems larger for cycle 6, with pressure oscillations of the order of 20–30 bars. An analysis is now proposed to investigate the correlation between the local pressure and heat release rate.

4.2.1. Analysis of cycle 6

Figure 10 presents the ΔP evolution on the horizontal plane during the AI sequence. The black line plotted on the ΔP fields represents an isoline of the AI progress variable which allows to locate AI spots. An isoline of the premixed flame progress variable (red) allows to follow the flame position.

At +19 CAD aTDC, the first AI spot starts in the upper right part of the combustion chamber (region A in Fig. 10a). A wave of a few bars amplitude is emitted and reflected on the chamber walls without coupling to the AI front. One CAD later, a second AI spot occurs (region B in Fig. 10b), still without coupling. After consumption of this spot, the combustion chamber presents no AI spots at 20.5 CAD aTDC (Fig. 10c). However one CAD later, at 21.5 CAD, a new AI spot appears in the bottom left part of the cut plane (region C in Fig. 10d). A particular attention should be paid to the image timing, because after Fig. 10d, the timing between two images is reduced to 0.1 CAD as AI propagates quickly in the chamber. An increase of the pressure wave amplitude is visible (Fig. 10d–h), and it reaches a value close to one hundred bars (whereas at ST = 8 CAD aTDC, amplitudes are about 1 bars). A correlation between the location of the pressure wave and the AI reaction rate is also visible for the first time. However, this AI spot is triggered late in the cycle, and the pressure wave begins to vanish after 21.9 CAD aTDC due to the lack of fuel to burn. The amplification of the wave seems to be a first sign of a deflagration to detonation transition, and corresponds to points located in the transition zone as suggested by Bradley's diagram in Fig. 5.

To make the analysis more quantitative, a circular 1D profile is plotted at three millimeters of the periphery of the combustion chamber as shown in Fig. 11 (black line). As the premixed flame already consumed the fresh gases in the center of the combustion chamber, this profile is assumed to be mainly in the fresh gases and perpendicular to the autoignition front propagation.

The pressure and AI reaction rate are plotted every angular degree (Fig. 12) on this profile looking for a correlation between AI reaction rate and pressure wave propagation. In addition, this figure also presents on the left the ΔP cut plane at the same instant and the detonation indicator $\mathbb{R}$ (Eq. (5)) on the right. At 21.5 and 21.6 CAD aTDC (Fig. 12a and b), an AI spot appears without clear coupling between the AI reaction rate and pressure peak. However, the AI reaction rate increases from 21.7 CAD aTDC (Fig. 12c) to 21.9 CAD aTDC (Fig. 12e), and its peak location and speed coincide now with the pressure wave whose amplitude reaches 180 bars in less than 0.5 CAD. A coupling is being established and this conclusion is coherent with the detonation indicator which reaches 1 in the region of coupling.

The previous observations are the first signs of a DDT. To ascertain these observations, the LES over-pressure and AI front velocity are now compared to those of an established detonation, given by Chapman–Jouguet (CJ) relations. The Chapman–Jouguet detonation velocity is given by:

$$D_{CJ} = \sqrt{2(\gamma^2 - 1) * Q} \tag{6}$$

where Q is the heat quantity generated by unit of mixture mass, and γ the ratio of specific heats fixed at 1.4. The Chapman–Jouguet pressure of burned gases is given by:

$$P_{CJ} \cong \rho_0 \frac{D_{CJ}^2}{\gamma + 1} \tag{7}$$

where ρ_0 is the local density in the fresh gases.

Using the present LES fresh gases conditions, D_{CJ} is estimated close to 2.3 km/s and P_{CJ} to 900 bars. On the other hand, the LES AI front velocity is estimated at about 1.1 km/s using the displacement speed of the maximum pressure peak between two images, and the maximum pressure variation reached at the

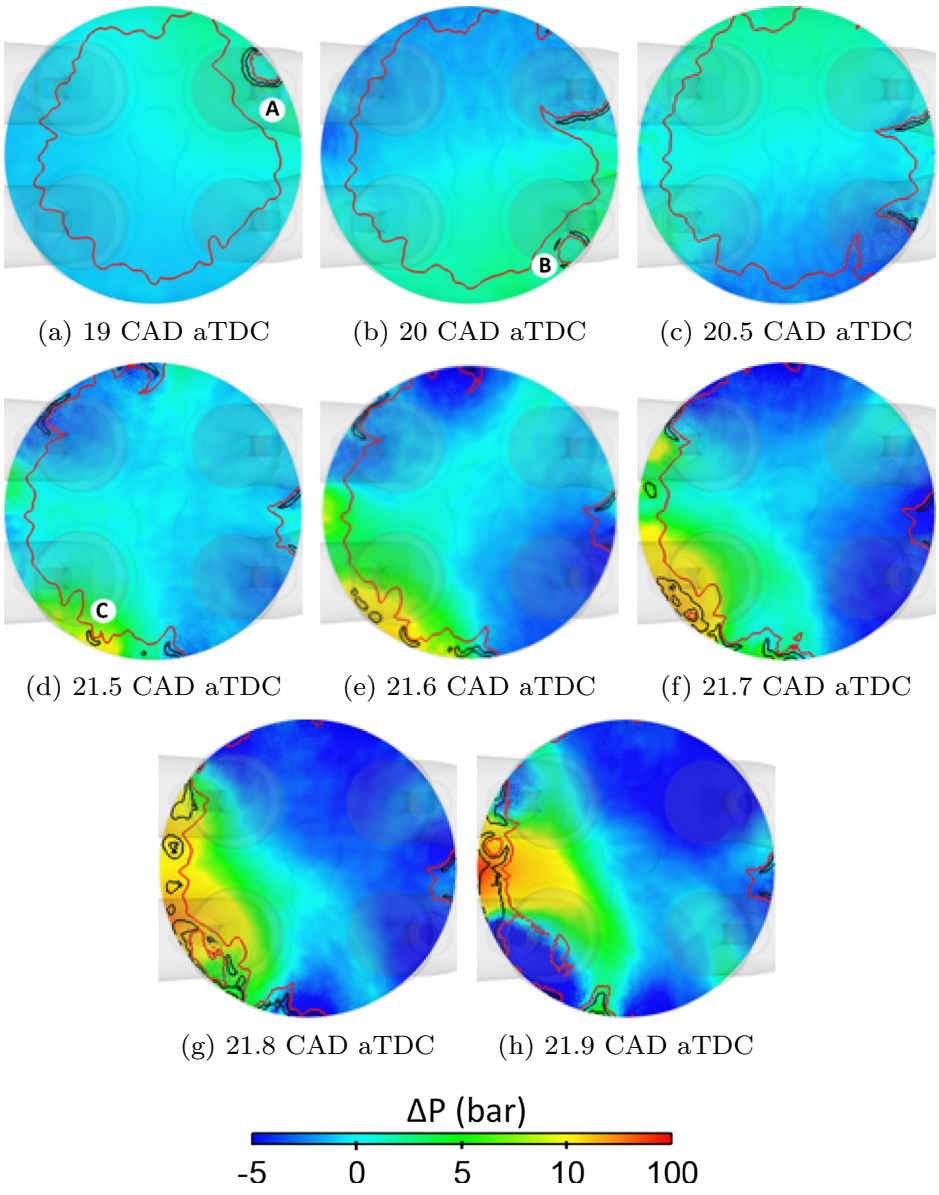

(a) 19 CAD aTDC (b) 20 CAD aTDC (c) 20.5 CAD aTDC

(d) 21.5 CAD aTDC (e) 21.6 CAD aTDC (f) 21.7 CAD aTDC

(g) 21.8 CAD aTDC (h) 21.9 CAD aTDC

Fig. 10. ΔP evolution for cycle 6 at ST = 0 CAD (Red line: isoline of c_Σ; Black line: isoline of c_{ai}). (For interpretation of the references to color in this figure legend, the reader is referred to the web version of this article.)

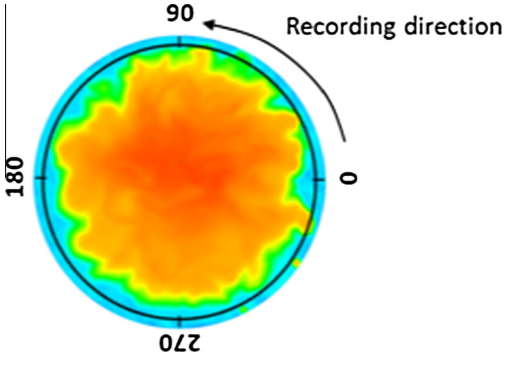

Fig. 11. 1D profile location (black line) on the observation plane.

same instant is close to 200 bars. These values are below the Chapman–Jouguet values but have the same order of magnitude, which indicates that a transition to detonation is observed and not a fully developed detonation. This transition is rapidly stopped in the LES due to a lack of fresh gases to feed the developing detonation. A second explanation for this difference is that Chapman–Jouguet theory assumes a one-dimensional detonation while the LES wave is not strictly one-dimensional. Finally, we note that both LES and Chapman–Jouguet values of the pressure variation are computed using the ideal gas law which is no more valid at such pressures. The discussed values must therefore be seen as approximations of the real pressure variations observed in the engine.

4.2.2. AI visualization of cycle 8

The same analysis is addressed for this new cycle. The first AI spot occurs at 23.75 CAD aTDC (2.75 CAD later than in cycle 6 at the same ST), and is visible in Fig. 13a (region A). A second AI spot starts nearly simultaneously (region B of Fig. 13b), but independently from the first one, at the opposite side of the chamber. It generates another pressure wave which travels in the opposite

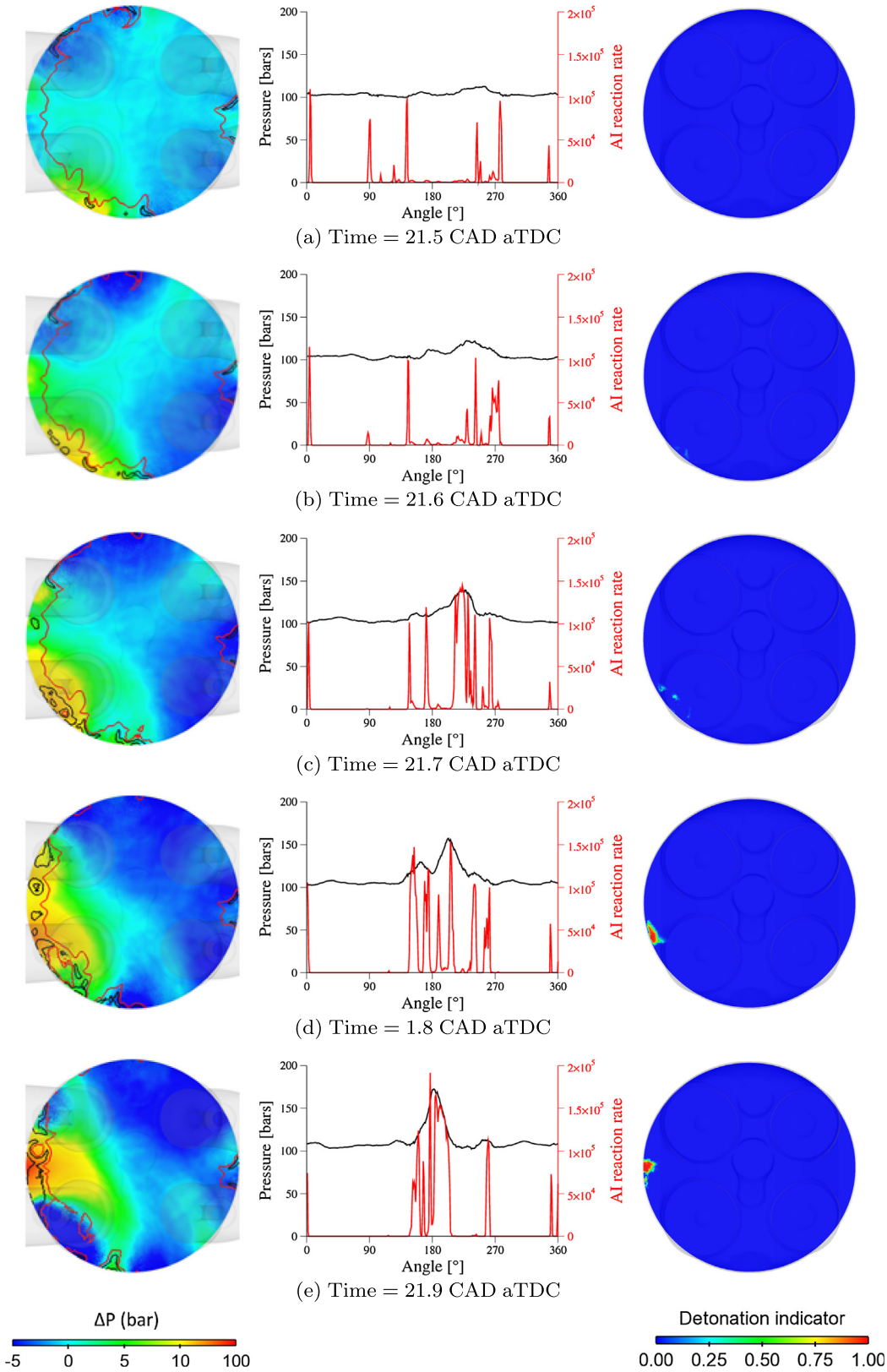

Fig. 12. ΔP evolution (left, red line: isoline of c_Σ; black line: isoline of c_{ai}), pressure and AI reaction rate on the 1D profile (middle) and detonation indicator (right) at several instants where a DDT is supposed for cycle 6 at ST = 0 CAD. (For interpretation of the references to color in this figure legend, the reader is referred to the web version of this article.)

direction (Fig. 13c). When these two waves collapse at 24.5 CAD aTDC (Fig. 13d), the overpressure generated initiates a third AI spot close to the wall (region C). This latter AI spot generates a stronger pressure wave which is reflected on walls (Fig. 13e–h), but without coupling to the AI reaction rate at any instants as the amplitude is low.

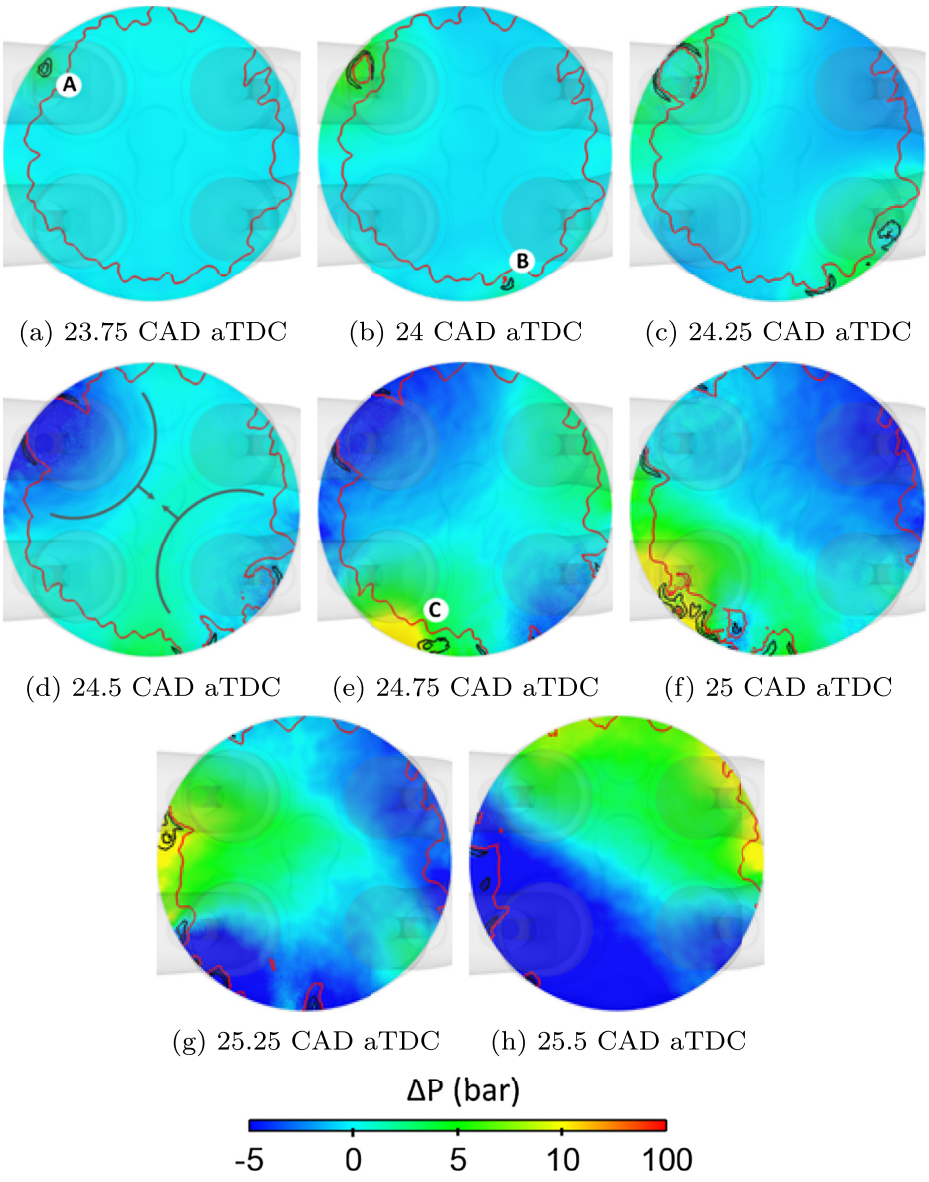

Fig. 13. ΔP visualizations for cycle 8 at ST = 0 CAD (Red line: isoline of c_Σ; Black line: isoline of c_{ai}). (For interpretation of the references to color in this figure legend, the reader is referred to the web version of this article.)

As for cycle 6, the pressure and AI reaction rate are displayed on a 1D profile in Fig. 14 to validate previous observations. In this case, no coupling is observed, and whatever the instant, the AI reaction rate peak is not correlated to the pressure peak. It is also important to notice that ΔP only reaches 10 bars, against 100 bars for the previous cycle. In the same way, the intensity of the AI reaction rate does not exceed 10^5 kg m^{-3} s^{-1} whereas for cycle 6 (Fig. 12) the value of the AI reaction rate doubles when it is reinforced by the pressure wave. Finally, the detonation indicator stays equal to 0 at any time, confirming that no coupling is present during this cycle.

4.2.3. Conclusions for spark timing cases at TDC

From the analysis of cycles 6 and 8, and from others not presented here, two scenarios were found at this ST. For cycles like cycle 8, no DDT was observed like for the ST of 8 CAD aTDC, leading to small amplitude pressure waves. On the contrary for cycles like cycle 6, the beginning of a DDT was clearly observed but it happened too late during the engine cycle to develop substantially. This DDT was evidenced by the coupling between the pressure wave and the fuel reaction rate, and by the characteristic pressure and velocity of this wave which are of the order of Chapman–Jouguet (CJ) values order of magnitude. In this case, the pressure wave reached a value of 100 bars, a value much larger than when no coupling is observed. Like for the previous ST, it was found that the detonation indicator is always in good agreement with the direct visualization analysis, that is, it has the ability to detect the presence of a DDT at the correct location and instant. These results confirm that this ST constitutes a transition point between the two extreme regimes pointed out in Fig. 4.

4.3. Super-knock

To study super-knock, two cycles with early spark timing (ST = 4 CAD bTDC) are chosen. Such an early ST compared to

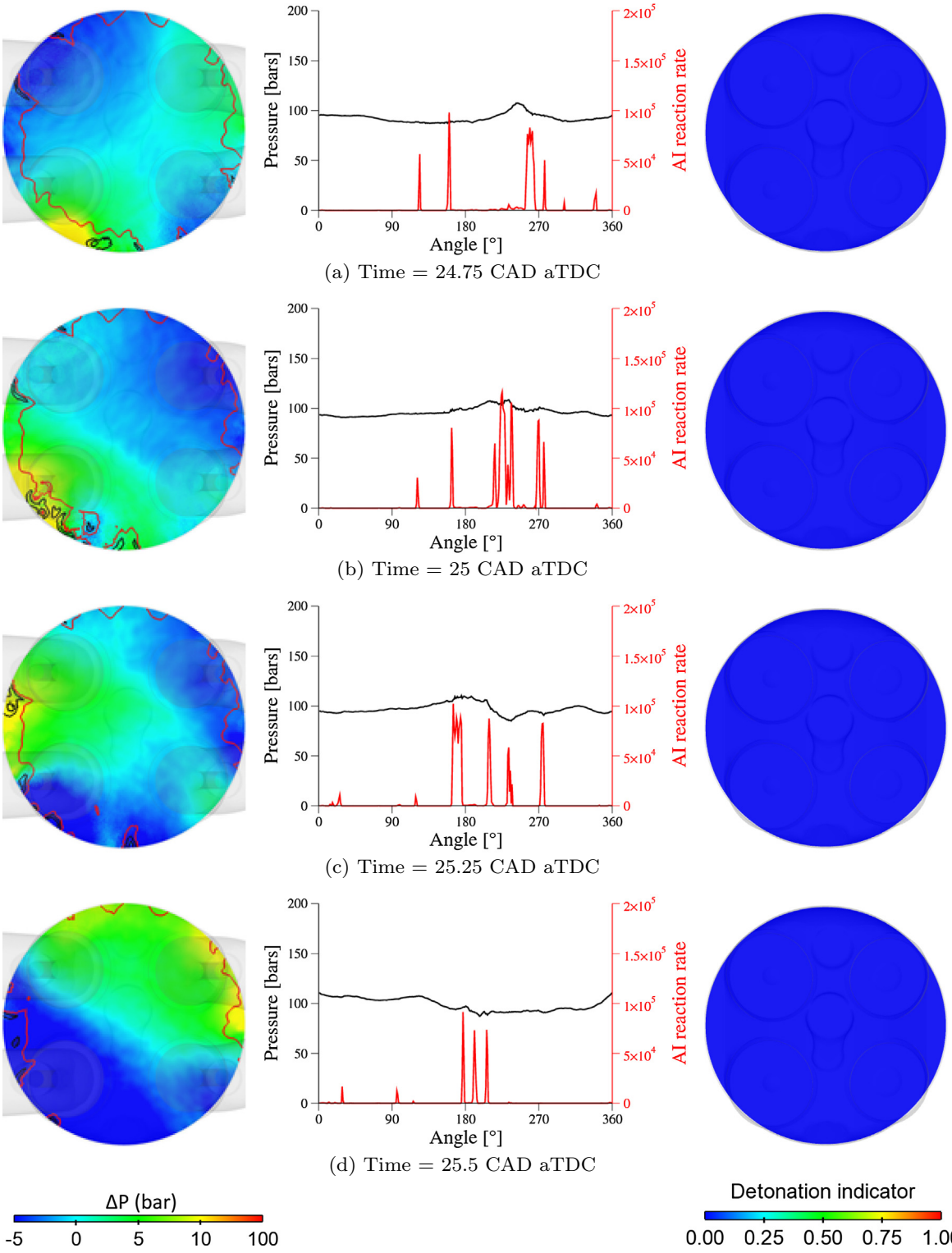

Fig. 14. ΔP evolution (left, red line: isoline of c_Σ; black line: isoline of c_{ai}), pressure and AI reaction rate on the 1D profile (middle) and detonation indicator $\mathbb{R}$ (right) for cycle 8 at ST = 0 CAD. (For interpretation of the references to color in this figure legend, the reader is referred to the web version of this article.)

the knock limit crank angle (fixed around 6 CAD aTDC for this engine) is not realistic, as it would lead to massive knock and engine destruction. It is solely used here, like in the experiment of Amann et al. [2], to mimic the creation of a premixed flame by a pre-ignition spot. Therefore, the autoignition events observed at this ST correspond to the ones observed in a cycle showing pre-ignition and not to a standard cycle. For cycles 7 and 8, the burned mass fraction (Fig. 15a) evolves in a nearly linear way when the propagation flame grows into the chamber after ignition. Around 10 CAD aTDC, the fuel consumption by the premixed flame tends to slow down, but at 13 CAD aTDC, a peak of AI reaction rate is observed for both cycles. This leads to a sudden increase of the burned mass fraction, and to the consumption of the 20% remaining fresh gases in only one CAD

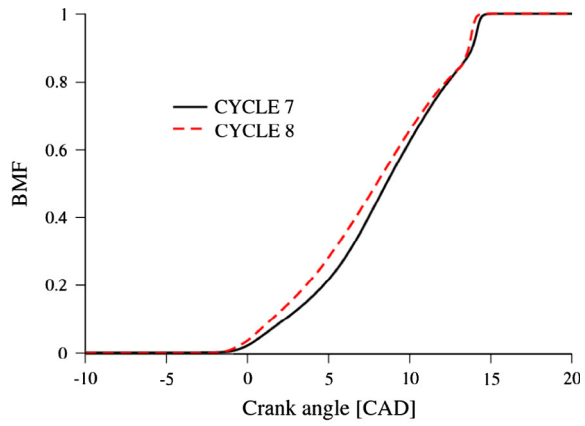

(a) Burned mass fraction over CAD

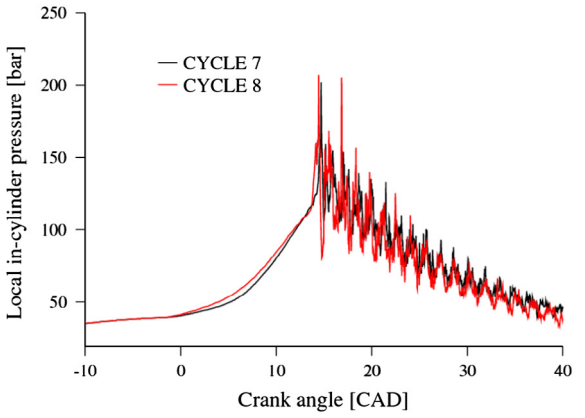

(b) Local in-cylinder pressure over CAD

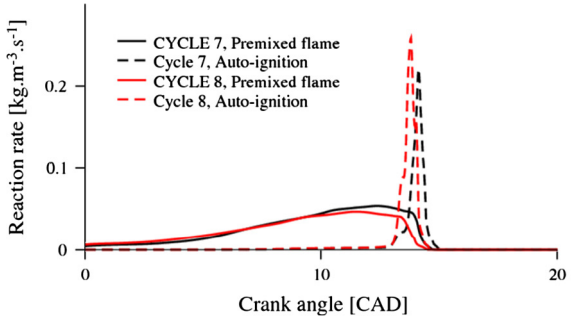

(c) Fuel reaction rates over CAD

Fig. 15. Burned mass fraction, local in-cylinder pressure and reaction rate evolutions for the LES cycles 7 and 8 at the ST = 4 CAD bTDC.

approximately. This increase of the consumption speed is more visible than for cycles with a ST at TDC, indicating a probably more intense coupling between the AI reaction rate and pressure waves compared to the previous cases.

4.3.1. Analysis of cycle 7

Figure 16 shows the evolution of ΔP on the horizontal plane at $z = 0$. AI starts at 13 CAD aTDC, and is visible at 13.2 CAD aTDC (Fig. 16a, region A). This AI spot of about 0.5 mm increases fresh gases temperature by only 5 K, and initiates a pressure wave which propagates into the chamber without reinforcing despite the two other AI spots visible at 13.8 CAD aTDC in Fig. 16c (region B and C). At this instant, the wave generated by the first AI spot impacts the opposite wall as illustrated by the arrow added to Fig. 16b. A new AI spot occurs at this location (Fig. 16d, region D) due to the overpressure generated, and a DDT is then visible in Fig. 16e–h, with an amplification of the wave that exceeds 200 bars (the legend is rescaled compared to the previous cycles analyzed). About 20% of the fresh gases remaining are finally consumed in about 1.2 CAD.

To analyze the physical mechanisms involved in this cycle, Fig. 17 presents the ΔP (left), fresh gases temperature (middle) and AI delay (right) evolutions during the presumed DDT occurence. The pressure wave impacts the wall at 13.9 CAD aTDC in region A (Fig. 17a) and generates an increase of the fresh gases temperature by more than 30 K which reduces locally the AI delay from a value of the order of 1 CAD down to 0.1 CAD approximately. This allows the creation of a new autoignition spot at this location which then grows and propagates towards the left as seen in Fig. 17b–e. During this growth, it can be noticed that the pressure front coincides with the autoignition reaction rate front (black isolines on the left column), fresh gases temperature increases and autoignition delay decreases. Inside the front, the AI delay typically takes values of the order of 0.1 CAD. Assuming a sound speed of 617 m/s corresponding to a fresh gases temperature of 950 K, the pressure wave only travels 5.7 mm before the AI delay is reached. This length scale is of the order of the size of the AI spot estimated close to 1 cm, thus indicating that a reinforcement of the pressure wave by AI can be expected, as effectively observed.

As presented for the previous ST, Fig. 18 shows at the same instants the 1D profiles of pressure (black) and AI reaction rate (red), along with 2D plots of ΔP (on the left) and of the detonation indicator (on the right). The correlation and propagation at the same velocity of ΔP and AI reaction rate peaks becomes more visible as time passes, confirming that a DDT is established. It can be noticed that the AI reaction rate peak is four times larger than for cycle 6 at ST = 0 CAD, where a DDT was already detected, and the maximum pressure peak is also more important with values close to 450 bars. In addition, looking at the detonation indicator, the regions where the indicator value equals 1 agree well with regions where a DDT is established (i.e. regions where ΔP is amplified).

The analysis of this cycle shows a scenario where the strong pressure wave is not generated by the first AI spot but by a secondary spot trigged by the initial spot. This scenario was inferred both experimentally and by a combustion analysis based on Bradley's theory [28]. It is here confirmed by LES which allows a detailed understanding of the physics at hand.

4.3.2. Analysis of cycle 8

Using the same analysis based on ΔP fields, a different scenario is pointed out for cycle 8 (Fig. 19). Large AI spots are first observed in region A of Fig. 19a, which generate a strong pressure wave. A coupling between ΔP and the AI reaction rate (black isoline) is observed on the left wing of the pressure wave that travels clockwise, between 13.5 and 14 CAD. It is similar to the coupling observed at cycle 7, whereas the right wing of the wave shows no reinforcement of the pressure wave (region B), probably due to a lack of fresh gases to consume. A new AI spot appears independently on the opposite side of the chamber (region C) at 13.6 CAD, and it also generates a pressure wave that travels counterclockwise and reinforces between 13.6 and 14 CAD. Finally, these two pressure waves merge at 14.1 CAD further increasing the pressure peak. As this AI sequence is very fast, the premixed flame displacement is small (red isolines in Fig. 19) during this period of time, which also means that the fresh gases are essentially oxidized by autoignition as confirmed by Fig. 15c.

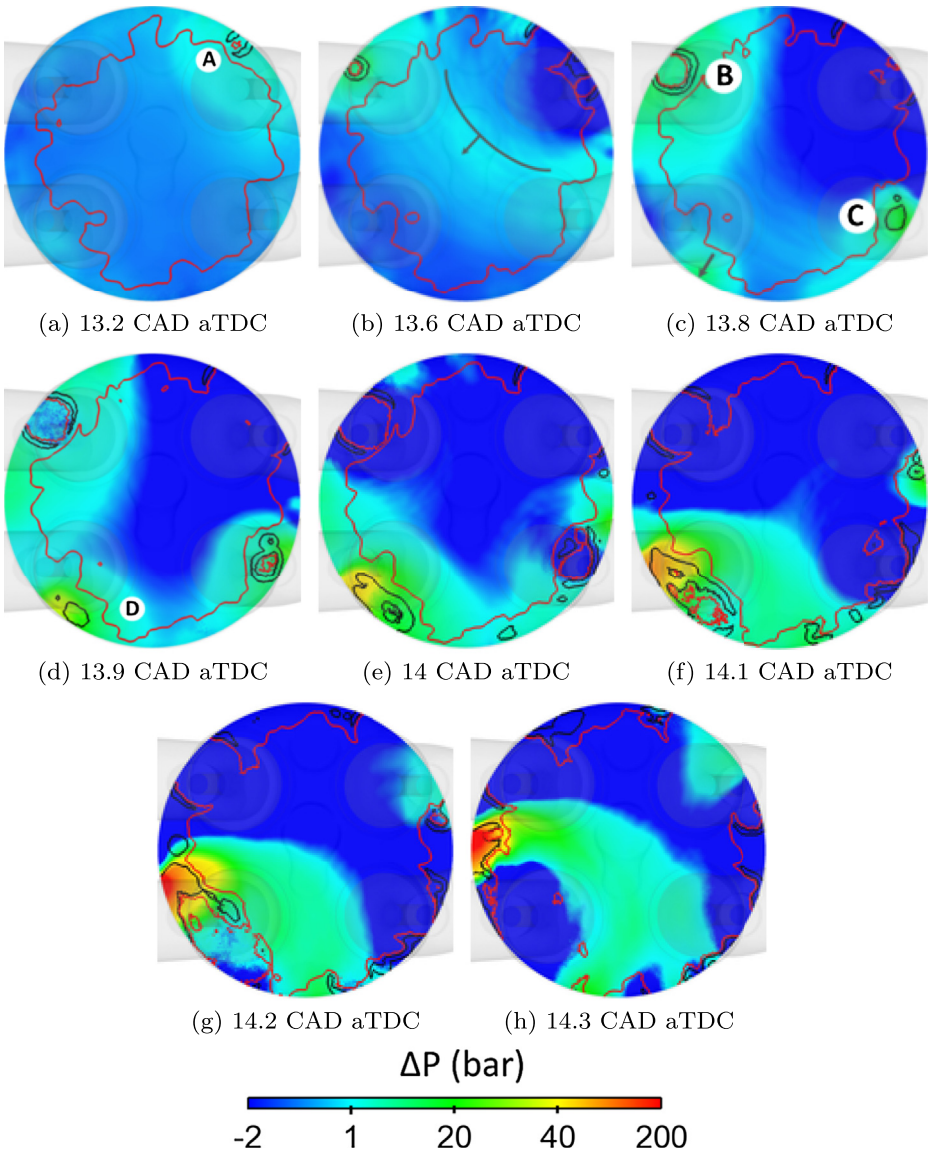

Fig. 16. ΔP visualizations for cycle 7 at ST = 4 CAD bTDC (Red line: isoline of c_Σ; Black line: isoline of c_{ai}). (For interpretation of the references to color in this figure legend, the reader is referred to the web version of this article.)

As for cycle 7, Fig. 20 compares the ΔP field (left), the pressure and reaction rate on 1D profiles (middle) and the detonation indicator (right) at five instants where coupling is visible in Fig. 19.

First of all, the 1D profiles between 13.3 CAD aTDC (Fig. 20a) and 14.1 CAD aTDC (Fig. 20e) confirm that a coupling is taking place in the region A, as the maximum pressure (black line) propagates at the same velocity as the AI reaction rate (red line). It is also observed that the peak pressure increases in this region from a couple of bars above the mean value at 13.3 CAD to approximately 400 bars at 13.9 CAD aTDC and even more at 14.1 CAD aTDC. At these two last crank angle degrees, the maximum pressure reached is higher than the constant volume pressure increase observed in a homogeneous autoignition in the same thermodynamic conditions, which is estimated at 319 bars. The velocity of the pressure wave can also be computed for this cycle looking at the displacement of the pressure peaks. It is estimated at about 1.5 km/s whereas, as a reminder, the Chapman–Jouguet velocity is estimated in such conditions at 2.29 km/s. The magnitude of the two velocities is quite close, which confirms the establishment of a DDT in such conditions.

A coupling is also observed in region C, although it is much less intense. When the two opposite travelling DDT waves from regions A and C collapse at 14.1 CAD, they induce a peak pressure close to 800 bars. This phenomenon was not observed in cycle 7 due to the existence of a sole DDT. Figure 20 confirms that region B does not lead to a DDT: except at 13.7 CAD where a small pressure increase can be observed, the pressure in this region remains very close to the mean pressure at all other times.

All these observations confirm that a DDT occurs during this cycle, and the detonation indicator $\mathbb{R}$ (right column of Fig. 20) succeeds in predicting the location and the time of appearance of DDTs in regions A and C, whereas it does not predict a DDT in region B (excepted at 13.7 and 14.1 in very small regions) in

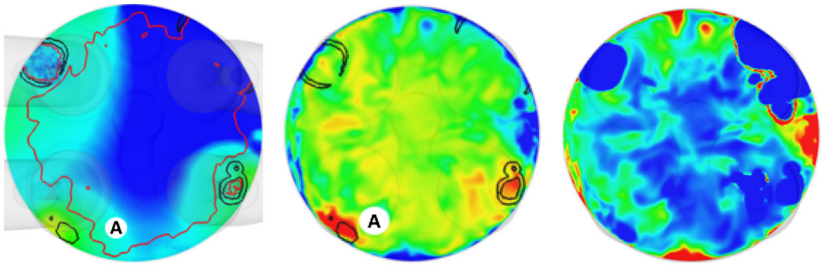

(a) Time = 13.9 CAD aTDC

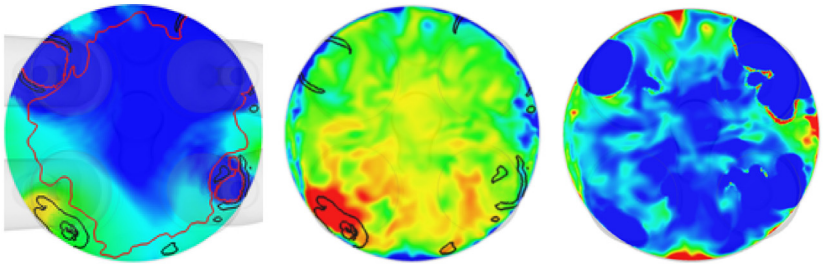

(b) Time = 14 CAD aTDC

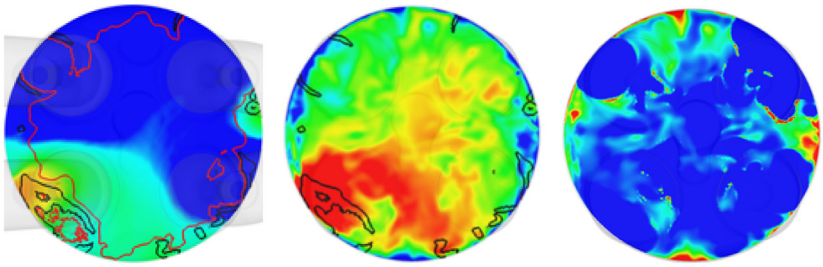

(c) Time = 14.1 CAD aTDC

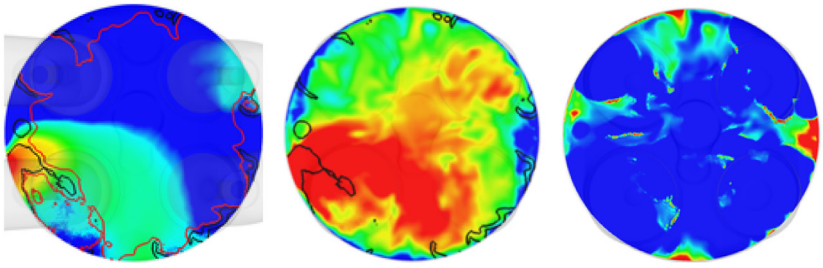

(d) Time = 14.2 CAD aTDC

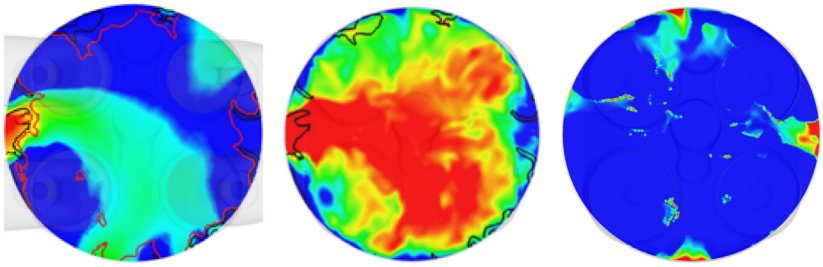

(e) Time = 14.3 CAD aTDC

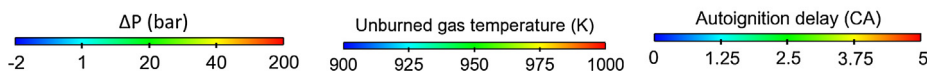

Fig. 17. ΔP evolution (left), fresh gases temperature (middle) and AI delay (right) at several instants where a DDT is supposed for cycle 7 at ST = 4 CAD bTDC (Red line: isoline of c_Σ; Black line: isoline of c_{ai}). (For interpretation of the references to color in this figure legend, the reader is referred to the web version of this article.)

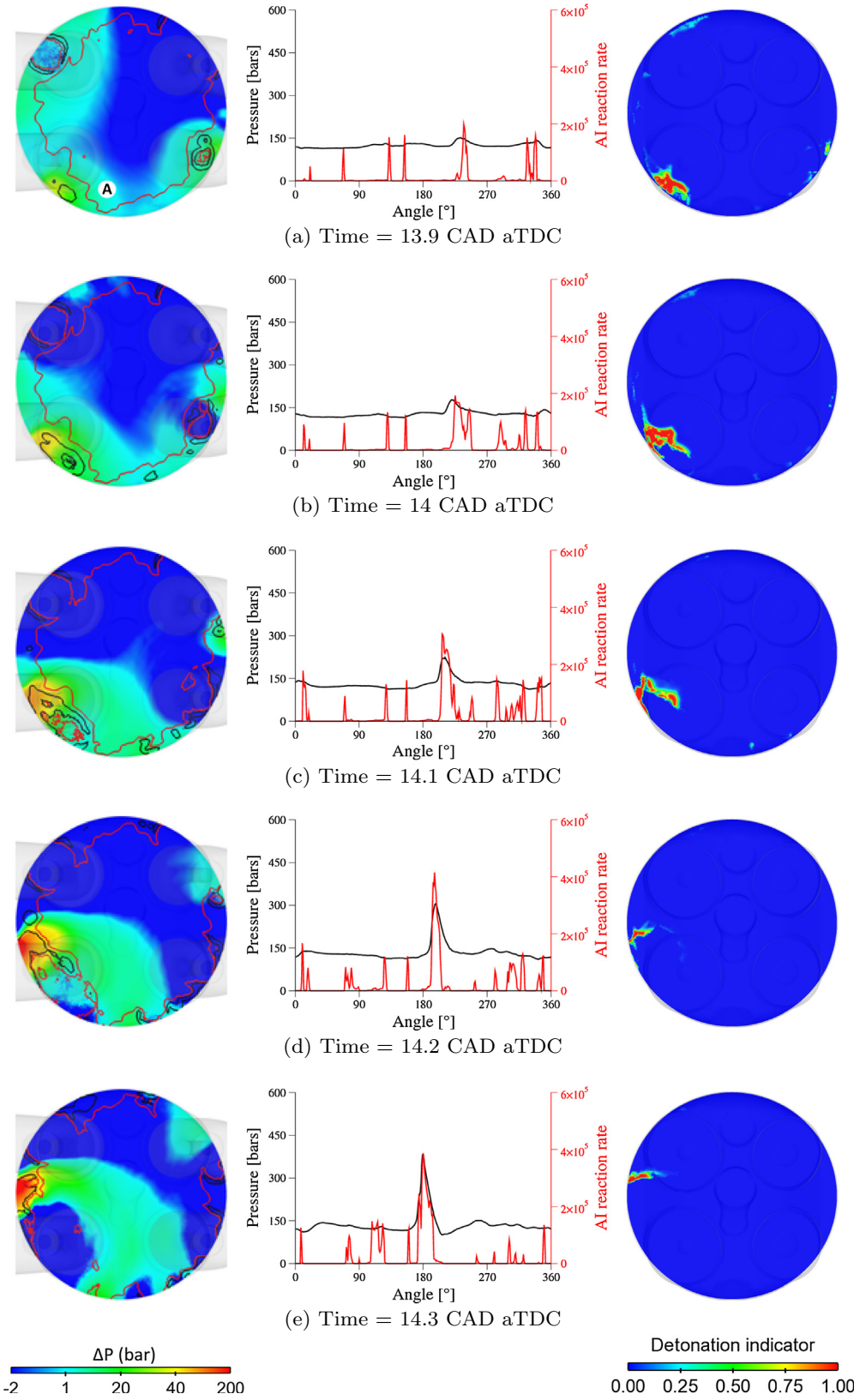

Fig. 18. ΔP evolution (left, red line: isoline of c_Σ; black line: isoline of c_{ai}), pressure and AI reaction rate on the 1D profile (middle) and detonation indicator (right) at several instants where a DDT is supposed for cycle 7 at ST = 4 CAD bTDC. (For interpretation of the references to color in this figure legend, the reader is referred to the web version of this article.)

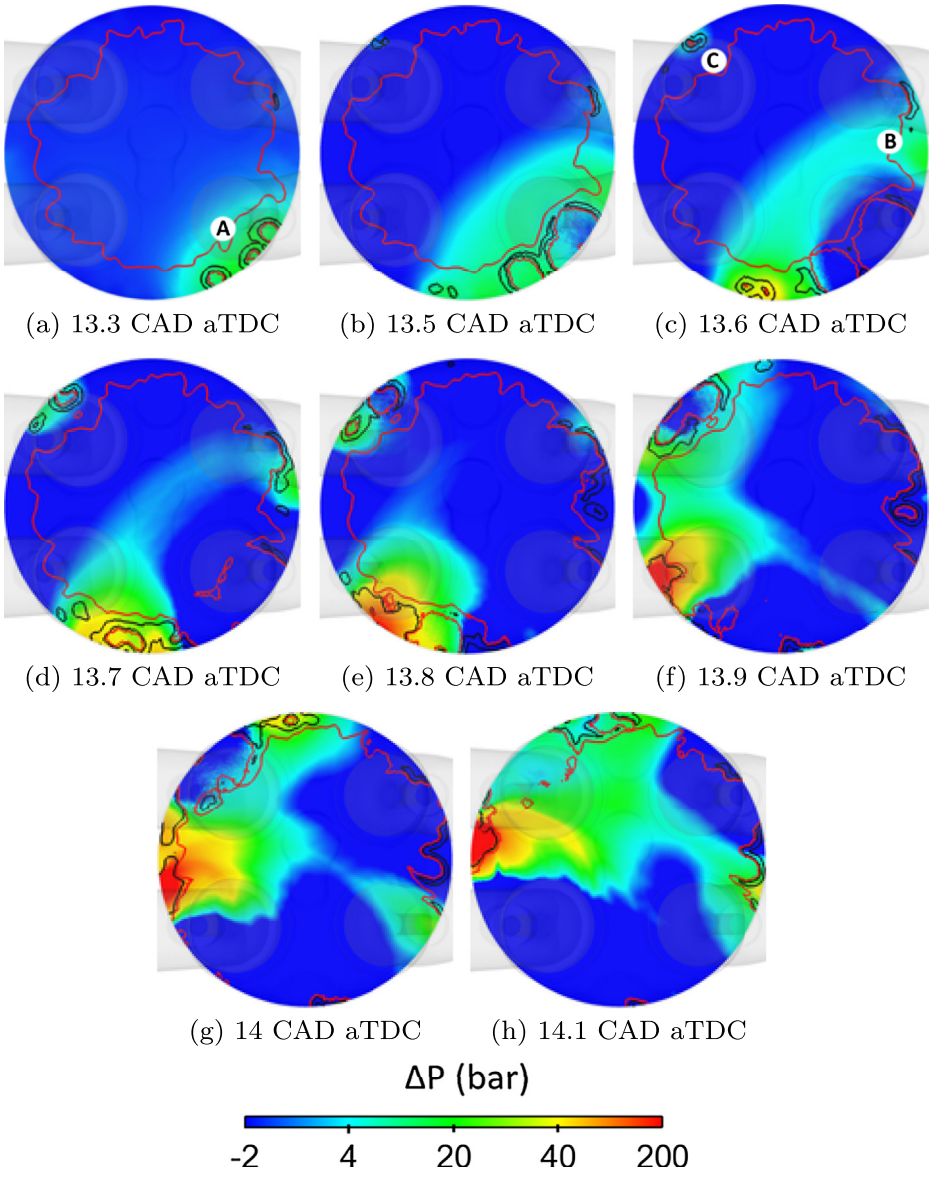

Fig. 19. ΔP evolution for cycle 8 at ST = 4 CAD bTDC (Red line: isoline of c_Σ; Black line: isoline of c_{ai}). (For interpretation of the references to color in this figure legend, the reader is referred to the web version of this article.)

agreement with the direct visualization. Fresh gases temperature and AI delay fields are not presented here but the same physical mechanisms as for cycle 7 are observed during this cycle. The three initial AI spots present a nearly spherical shape with a radius of the order of 0.6 mm. Within these spots the fresh gases temperature increases by 30 K approximately at the instant of autoignition, and these spots generate a strong pressure wave during the heat-release period. The propagation of this wave implies an increase of fresh gases temperature and a decrease of the AI delay, allowing AI to start before the pressure wave had time to propagate away from the reaction zone.

Finally, this LES also shows that the piston is submitted locally to drastic thermodynamic conditions which can explain some real engine damages after pre-ignition events. The limit of an abnormal combustion analysis relying only on local in-cylinder pressure sensors is thus pointed out: during this cycle, the local pressure sensor shows (Fig. 15b) strong fluctuations, but the maximum pressure recorded does not exceed 210 bars, which is far from the 800 bars recorded locally at other locations. It can be concluded that performing a knock analysis based only on a local sensor (or a couple of sensors) makes the result very dependent on the relative distance between the AI spot and the sensor location.

4.3.3. Conclusions for ST = 4 CAD bTDC

LES analysis shows that the exponential increase of the knock intensity observed at this ST (Fig. 4) is due to a coupling between the pressure wave and the local autoignition. This interaction produces a pressure which is much larger than the final constant volume pressure that would be observed during a thermal explosion.

It also explains why the quantity of fresh gases mass burned by AI is not sufficient to explain alone such high intensities. LES allows identifying this coupling explicitly because local and instantaneous conditions of pressure and temperature are directly resolved on the CFD mesh, unlike in RANS or in experiments.

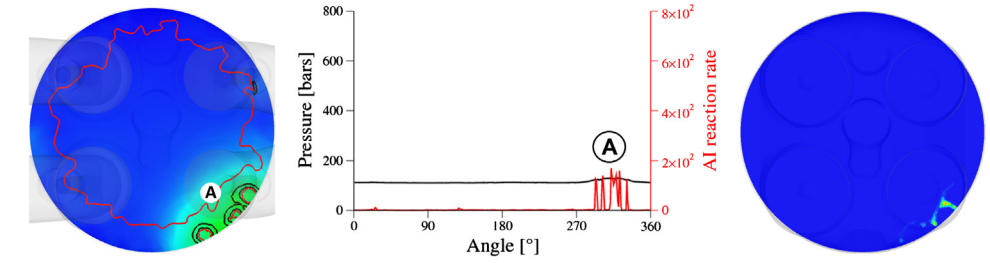

(a) Time = 13.3 CAD aTDC

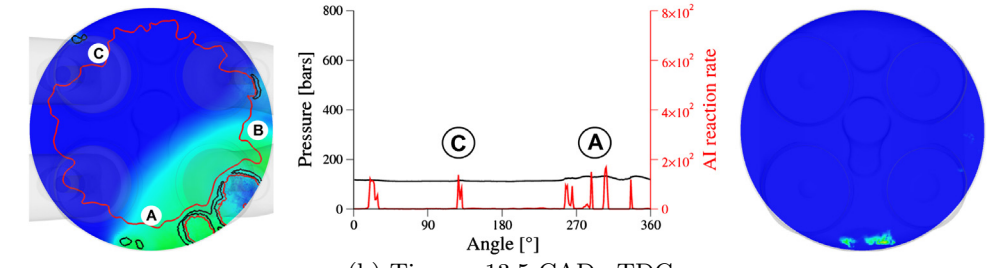

(b) Time = 13.5 CAD aTDC

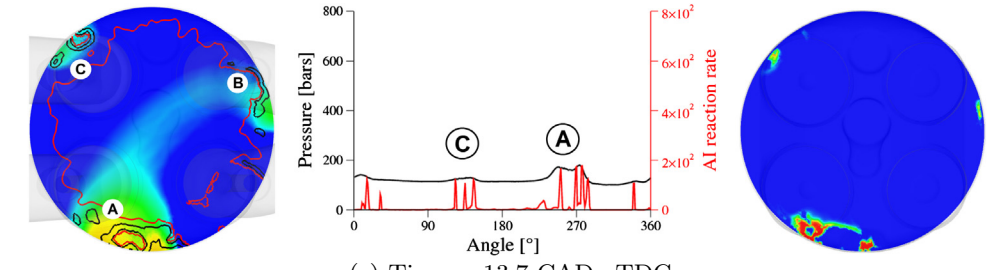

(c) Time = 13.7 CAD aTDC

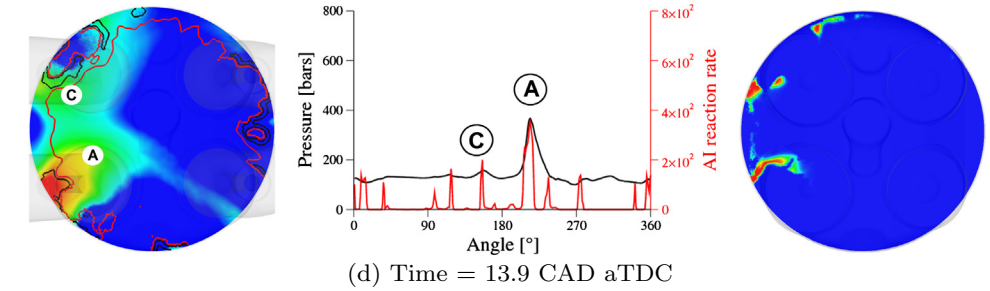

(d) Time = 13.9 CAD aTDC

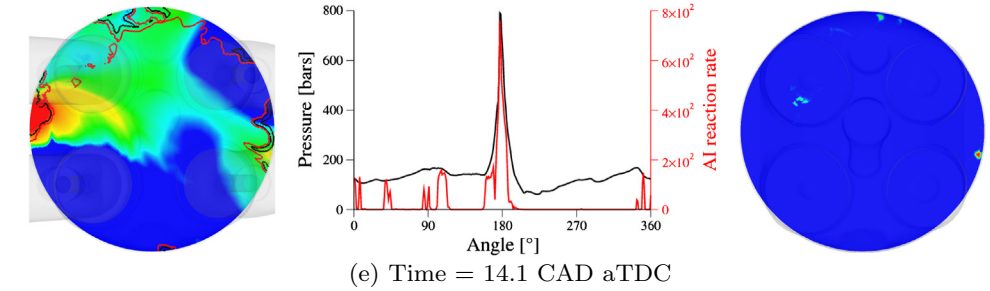

(e) Time = 14.1 CAD aTDC

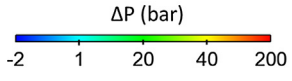

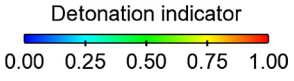

Fig. 20. ΔP evolution (left, red line: isoline of c_Σ; black line: isoline of c_{ai}), pressure and AI reaction rate on the 1D profile (middle) and detonation indicator (right) at several instants where a DDT is established for cycle 8 at ST = 4 CAD bTDC. (For interpretation of the references to color in this figure legend, the reader is referred to the web version of this article.)

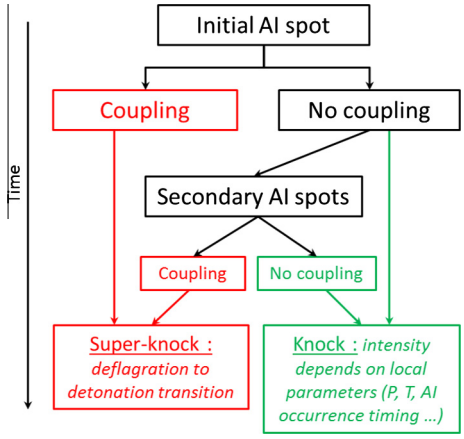

Fig. 21. Schematization of AI scenario visualized in LES calculations.

5. Conclusions

A first LES study addressing different scenarios for knock and super-knock observed in a SI engine is presented in this article. Based on the evolution of knock intensity against the mass burned by AI, two regimes are observed: at low knock intensities, corresponding to standard spark timing, knock intensity is found proportional to the mass burned by AI. For the earliest ST on the contrary, corresponding to super-knock, knock intensity is still found proportional to the mass burned by AI but with a much stronger slope, suggesting a drastic change in the phenomena at stake. The literature suggests that this regime is in fact a deflagration to detonation transition. To contribute to elucidate this question, two analyses are proposed, both based on multi-cycle LES of a SI engine operating point at different ST. The first one is "a priori": it applies Bradley's diagram to the instantaneous LES fields. The second one is "a posteriori": it consists in analyzing directly the LES fields to figure out if a coupling between the pressure waves and the autoignition reaction rate is observed or not.

The a posteriori analysis allowed to identify different scenarios of AI. Figure 21 sums up these scenarios starting on the top from the necessary condition: having a first AI spot. Consequences can be different in terms of AI intensity (and pressure level), because each AI spot can couple or not with the generated pressure wave. Two regimes could be identified:

- The lowest intensities (green in Fig. 21) are linked to one or several local AI spots which consume the surrounding fresh gases within a few centimeters around the initial spot. There is no coupling with the initial pressure wave, which is only reflected on the chamber walls. These pressure fluctuations are well captured by the local in-cylinder pressure sensor, and their amplitude depends on the timing of AI event during the cycle, i.e., on the quantity of fresh gases available, and the local thermodynamic conditions. This case corresponds to a low to moderate knock intensity as encountered for knocking cycles after a normal flame ignition by the spark plug.
- The highest intensities (red in Fig. 21) correspond to what is usually called super-knock, a very intense knock observed under pre-ignition conditions or for very early ST, as done in this study. LES shows that the pressure waves generated by one or a couple of AI spots are strong enough to induce an increase of the fresh gases temperature which is itself strong enough to substantially decrease the AI delay. This allows to generate a coupling between the pressure wave and the AI reaction rate which reinforce each other. The maximum pressure reached by the reactive wave can be much larger than the one reached in a constant volume vessel at the same thermodynamic conditions. These results allow to identify these cases as deflagration to detonation transitions. It therefore strongly supports the hypothesis proposed in the literature [12,28] that super-knock is caused by deflagration to detonation transition.

Thanks to the use of a local detonation indicator $\mathbb{R}$ based on Bradley's diagram, it is finally shown that this a priori tool not only predicts the change of combustion regime as a function of the ST, but it also roughly succeeds in predicting the location and time of appearance of the DDT in the chamber. Unfortunately, as suggested by Fig. 21, the first AI spot is not always responsible for the DDT. This means that using cold flow LES to calculate the detonation indicator instead of a reacting LES as proposed here, would lead to a failure of the indicator in many cases.

Acknowledgments

This work was partly funded by the Agence Nationale de la Recherche (ANR) in the ICAMDAC projet (ANR-10-VPTT-002). It was granted access to the High Performance Computing (HPC) resources of CCRT under the allocations c2013-026139 and x20142b6139 made by GENCI (Grand Equipement National de Calcul Intensif).

References

[1] K. Steurs, C. Blomberg, K. Boulouchos, SAE Int. J. Engines 7 (2014) 1752–1772.
[2] M. Amann, D. Mehta, T. Alger, SAE Int. J. Engines 4 (2011) 274–285.
[3] F. Vangraefschepe, J. Zaccardi, in: SIA Conference Strasbourg, 2007.
[4] P. Haenel, P. Seyfried, H. Kleeberg, D. Tomazic, SAE Technical Paper, 2011-01-0343.
[5] N. Kawahara, E. Tomita, Int. J. Hydrogen Energy 34 (2009) 3156–3163.
[6] M. Katsumata, K. Morikawa, M. Tanabe, SAE Technical Paper, 2011-01-1875.
[7] E. Corti, C. Forte, SAE Int. J. Engines 2 (2009) 368–380. 2009-24-0019.
[8] F.-A. Lafossas, M. Castagne, J.P. Dumas, S. Henriot, SAE Paper 2002-01-2701.
[9] J. Shao, C. Rutland, SAE Technical Paper, 2014-01-1221.
[10] B. Reveille, A. Duparchy, Oil Gas Sci. Technol. – Rev. IFP Energies nouvelles 64 (3) (2009) 431–444.
[11] D. Linse, A. Kleemann, C. Hasse, Combust. Flame 161 (4) (2014) 997–1014.
[12] N. Peters, B. Kerschgens, G. Paczko, SAE Int. J. Engines 6 (2013) 953–967. 2013-01-1109.
[13] A. Robert, S. Richard, O. Colin, L. Martinez, L.D. Francqueville, Proc. Combust. Inst. 35 (3) (2014) 2941–2948.
[14] D. Bradley, C. Morley, SAE Technical Paper, 2002-01-2868.
[15] X. Gu, D. Emerson, D. Bradley, Combust. Flame 133 (1–2) (2003) 63–74.
[16] D. Bradley, G. Kalghatgi, Combust. Flame 156 (12) (2009) 2307–2318.
[17] G.T. Kalghatgi, D. Bradley, Int. J. Engine Res. 13 (4) (2012) 399–414.
[18] V. Moureau, G. Lartigue, Y. Sommerer, C. Angelberger, O. Colin, T. Poinsot, J. Comput. Phys. 202 (2) (2005) 710–736.
[19] O. Vermorel, S. Richard, O. Colin, C. Angelberger, A. Benkenida, D. Veynante, Combust. Flame 156 (8) (2009) 1525–1541.
[20] O. Colin, K. Truffin, Proc. Combust. Inst. 33 (2) (2011) 3097–3104.
[21] O. Colin, A.P. da Cruz, S. Jay, Proc. Combust. Inst. 30 (2005) 2649–2656.
[22] N. Branley, W.P. Jones, Combust. Flame 127 (2001) 1914–1934.
[23] G. Lecocq, S. Richard, J.-B. Michel, L. Vervisch, Proc. Combust. Inst. 33 (2) (2011) 3105–3114.
[24] S. Jerzembeck, N. Peters, P. Pepiot-Desjardins, H. Pitsch, Combust. Flame 156 (2) (2009) 292–301.
[25] S. Butterworth, Wireless Eng. 7 (1930) 536–541.
[26] G.A. Karim, SAE Technical Paper, 2004-01-1992.
[27] S. Richard, S. Bougrine, G. Font, F.-a. Lafossas, F. Le Berr, Oil Gas Sci. Technol. – Rev. IFP Energies nouvelles 64 (3) (2009) 223–242.
[28] J. Rudloff, J.-M. Zaccardi, S. Richard, J. Anderlohr, Proc. Combust. Inst. 34 (2013) 2959–2967.
[29] G.T. Kalghatgi, Proc. Combust. Inst. 35 (2015) 101–115.
[30] Y. Zel'dovich, Combust. Flame 39 (2) (1980) 211–214.